ABSTRACT

Title of dissertation: IMPLEMENTATION OF E-BEAM
PROXIMITY EFFECT CORRECTION
USING LINEAR PROGRAMMING
TECHNIQUES FOR THE FABRICATION
OF ASYMMETRIC BOW-TIE ANTENNAS

Filiz Yesilkoy, Master of Science, 2010

Dissertation directed by: Professor Martin Peckerar
Department of Electrical
and Computer Engineering

Asymmetric nano-bow-tie antennas offer the possibility of direct light-to-electrical energy conversion. These nano-antennas are easily integrated with conductor-barrier-conductor (CBC) tunnel junctions in between the antenna segments for the purpose of coupled signal rectification. The architecture of the tunnel junction together with the antenna size precision require nano-scale patterning accuracy. Electron Beam Lithography (EBL) is used for patterning purposes. In this study Proximity Effect (PE), a very common resolution problem in EBL, is reduced by a dose modulation technique employing linear programming (LP) algorithms. Production of tightly controlled antenna segment dimensions is achieved in conjunction with a small area tip and a small tunnel junction gap. It is expected that precise control of the gap geometry will enhance detection speed, enabling the utilization of the device for the visible range energy harvest purposes.

IMPLEMENTATION OF E-BEAM PROXIMITY EFFECT CORRECTION USING LINEAR PROGRAMMING TECHNIQUES FOR THE FABRICATION OF ASYMMETRIC BOW-TIE ANTENNAS

by

Filiz Yesilkoy

Thesis submitted to the Faculty of the Graduate School of the
University of Maryland, College Park in partial fulfillment
of the requirements for the degree of
Master of Science
2010

Advisory Committee:
Professor Martin Peckerar/Advisor
Professor Neil Goldsman
Professor Mario Dagenais

Table of Contents

Chapter 1

Introduction

As improvements in the technology allow nanometric precision in feature dimensional tolerances, new devices have been discovered. Recently, nano-size optical antennas have been receiving great attention, inspired by their radio-frequency counterparts. The thin film planar type antenna coupled conductor-barrier-conductor (CBC) tunnel junction is an example of nano-size optical antennas which offer great advantages in various application areas like tunable antennas and light detection in the infrared to visible range of the spectrum. However, the architecture of this device needs unprecedented control over feature shapes and dimensions, stressing even modern day process technology. This thesis focuses on the fabrication of thin film planar type antenna coupled CBC tunnel junctions using Electron Beam Lithography (EBL). We aim to improve the common resolution problem of EBL called Proximity Effect (PE). A brief description of the device structure and the details of the research performed to improve the fabrication process will be given.

1.1 Description of antenna coupled CBC tunnel junctions

Antenna-coupled CBC tunnel junction diodes offer great advantages for the detection of high frequency electromagnetic waves up to the visible range owing to their high speed of response. The operational structure of this device can be broken

into two parts. The first part is the antenna where the incident light is coupled forming an AC signal across the antenna parts. Rectification of this AC signal is necessary for the detection of the incident light as a manageable signal. As a result of this, the coupled signal is rectified in the second part of the device, which is a tunnel junction that converts the AC signal into a DC signal across the two conductor segments of the antenna.

Optical antennas can be formed either by mimicking radio-frequency antennas with smaller dimensions, or by creating new designs that will satisfy the necessary requirements. For our applications a variation of a bow-tie antenna called an "asymmetric bow-tie" shown in figure 1.1 is preferred. One reason why this type is preferred is that bow-tie antennas have a broader bandwidth than the simple dipole and its variants. This gives bow-ties sensitivity over a broader spectrum of the incident radiation. They are also robust in the face of dimension inaccuracy created during manufacturing. Furthermore, the selected antenna design is very appropriate for downscaling the dimensions to bring the target frequency band into the infrared(IR) and possibly visible range.
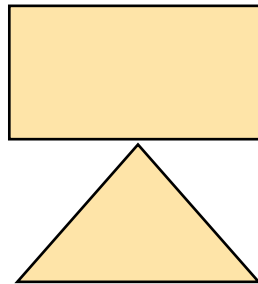
Figure 1.1: Asymmetric Bow-Tie Antenna Pattern

Bow-tie antennas are capable of vigorously concentrating electric field in the gap formed in between two conductive antenna parts when a correctly polarized electromagnetic wave at the proper wavelength is incident on them. There are several aspects contributing to this field confinement phenomena. The first and the most obvious (for our structure) is the "lightning rod effect" created by the sharp point of the cathode of the CBC diode embedded in the bow-tie antenna. Another important contribution comes from the resonance of surface plasmon polaritons. At optical frequencies, the incident wave causes oscillations in the free electron sea of the metal surface. These surface oscillations, called surface plasmons, when brought to a resonance cause the maximum accumulation of opposite charges on the opposite sides of the antenna arms, triggering the confinement of the electric field at the antenna gap. The surface plasmon resonance in the antenna is achieved if the length of the antenna arms are an odd integer number of half surface plasmon wavelengths ($L_{res} = n\lambda/2$). Together with the traditional antenna resonance, surface plasmons create a massive sub-wavelength electric field enhancement at the antenna gap. In order to achieve the plasmonic, as well as the "lightening rod" enhancement effect, the polarization of the electric field vector must point in the direction to desired electron transport. If the antenna arms are suspended, one above another, the plasmon polarization vector falls (at least partly) in the direction normal to that of the desired transport. This physical phenomena imposes single layer fabrication restriction on our antenna design. This is one of the biggest challenges to our work.[12] [43]

In the asymmetric bow-tie optical antenna structure, rectification is realized by

the built-in CBC tunnel junction where the conductor parts are formed by the metal antenna sections and the barrier is at the gap in between these antenna parts. A very common characteristic of CBC structure is the nonlinear I-V (current-voltage) behavior across its conductor portions. This nonlinear I-V characteristic creates rectification and the DC signal associated with that rectification is expressed below in equation 1.1 [14]. According to this equation the magnitude of the signal formed is proportional to the second derivative of the I-V curve and the amplitude of the AC signal coupled. For a high rectification efficiency high curvature in the I-V curve is required.

$$V_{dc} \propto \frac{1}{4} \frac{d^2 I}{dV^2} \triangle V^2 \tag{1.1}$$

There are various physical factors playing an active role in the formation of the nonlinear I-V behavior. The first and foremost is electron tunneling, which can be defined as the classically forbidden transport of electrons through the barrier shown in figure 1.2 a) below. According to quantum mechanics, tunneling probability increases exponentially as the barrier thickness decreases. Therefore, the success of the rectification strongly depends on the physical barrier thickness. Moreover, the field enhancement at the gap forms the bias voltage across the barrier shown in figure 1.2 b), which also plays an important role in defining the barrier thickness by shrinking the physically determined barrier width. Another mechanism that contributes to the nonlinearity in the I-V relation is the thermionic emission. Briefly,

this phenomena can be described by electron ejection over the barrier caused by the thermal excitement created by the temperature increase in the material. Although thermionic emission creates a considerable contribution to the nonlinearity, this conduction mechanism is not as effective as tunneling for the high frequency detection because thermal excitation is a slow process compared to tunneling [9].
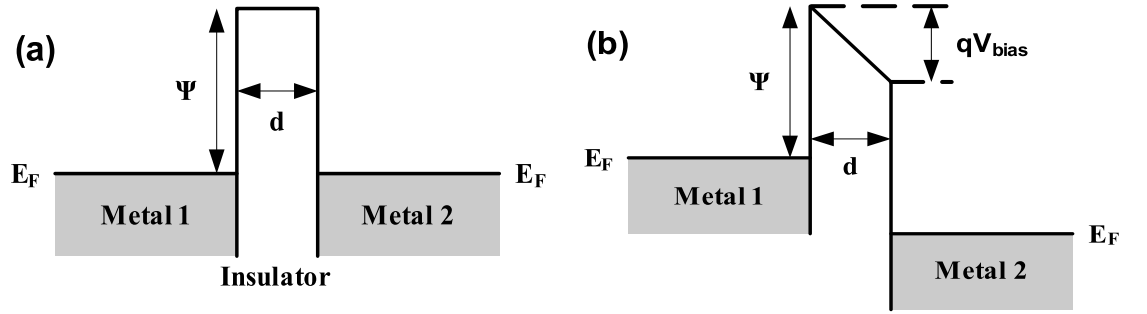
Figure 1.2: Tunnel junction diode energy band structure (a) before (b) after the potential difference is applied

The most important prerequisite for IR and visible light detection is a detector RC time constant shorter than one wave cycle of the light to be detected. As indicated above, the tunneling mechanism does not bring a restriction because its cut-off frequency is much higher than the required. However, the equivalent circuit of this device features a junction capacitor across the barrier (C_d) and an antenna resistance R_a in series with the junction capacitance. This introduces a time constant and defines the cut-off frequency limit given in equation 1.2. It is clear from the equation that in order to assure a high cut-off frequency (and therefore a fast response time) a small junction capacitance is required. Equation 1.3 defines the

junction capacitance taking the junction as a parallel plate capacitor. In this equation ϵ and ϵ_0 are relative electric permittivity and the permittivity of free space, respectively; A represents the junction area, and d stands for the distance between the conductor surfaces. Based on this equation, it is necessary to create a small junction area and a large distance between the plates to form a small C_D. However, since a large distance between the plates affects the tunneling mechanism, the only free variable to maintain a high cut-off frequency is the junction area.

$$V_c = \frac{1}{2\pi R_A C_D} \tag{1.2}$$

$$C_D = \varepsilon\varepsilon_0 \frac{A}{d} \tag{1.3}$$

1.2 Previous work on antenna coupled CBC tunnel junctions

The first generation CBC diodes were first reported as point contact Metal-Oxide-Metal (MOM) diodes working at millimeter and sub-millimeter wavelengths as shown in figure 1.3 [7]. These devices are composed of a metal wire acting as an antenna and a MOM diode formed at the sharp tip of the wire touching the oxidized surface of another metal. Although first generation MOM diodes had considerably high speed response abilities due to their very small diode contact area, they lacked stability and reproducibility due to poor mechanical properties. Hence, the second generation thin-film MOM diodes came into play in the early seventies [38] [40] [13]. This approach allowed the implementation of the antenna and the tunnel junction by integrating them on a substrate using lithography. An

example of the second generation devices that use bow-tie shape antenna is shown in figure 1.4. Although integrated devices brought stability and reproducibility, their performance was restricted by integrated circuit fabrication technology. Progress here had to follow the evolution in lithography. Second generation antenna-coupled MOM diodes were first implemented by photolithography and then EBL, which enabled the fabrication of smaller area junctions, and thus increased the frequency range of the detectable electromagnetic waves from microwave to IR.
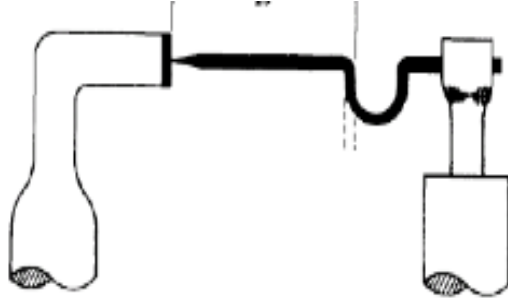
Figure 1.3: First generation point contact MOM diodes [7]

The work we present here concerns the third generation of antenna-coupled CBC diodes. These devices are fabricated by patterning a single thin conducting layer using EBL. The principal difference between the second and the third generation is the manner the CBC tunnel junction is formed. In the second generation the tunnel junction is constructed vertically by overlapping two metal layers, one on top of another, with the oxide tunnel layer in between. In the third generation device, the junction is formed horizontally in between two planar metal sections of the antenna. This will enable the utilization of the prominent electric field confined
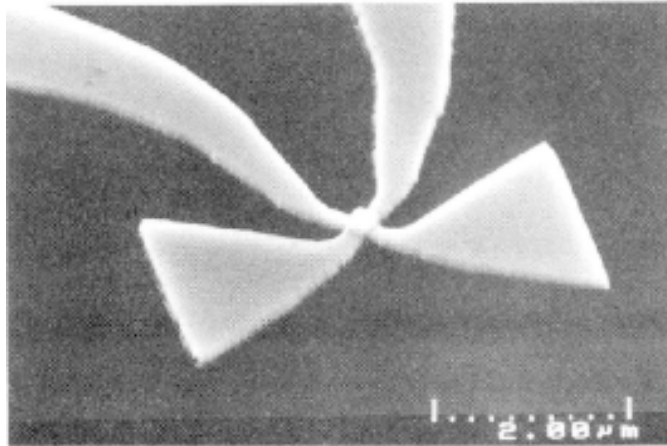
Figure 1.4: Second generation point contact MOM diodes [3]

across the junction to enhance the tunneling actions. Figure 1.5 shows an example

of the third generation fully planar device [18].
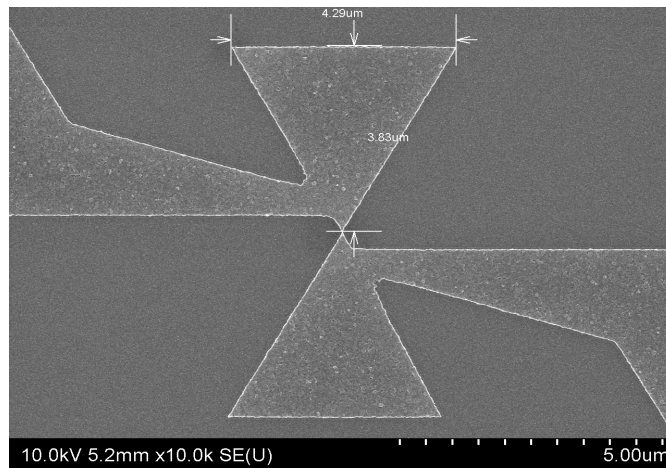
Figure 1.5: Third generation tunnel junction diodes

1.3 Objectives and challenges

The third generation antenna coupled CBC tunnel junction devices have offered various improvements in the performance of optical antennas. Increase in the cut-off frequency enabled the detection of a larger range of electromagnetic waves. In addition, the planar structure allowed the use of surface plasmons. Therefore, a planar single layer fabrication process where the tunnel junction is formed in a horizontal manner became essential. This new approach led to several challenges because its success strongly depends on the lithography resolution limitations.

The first and the foremost challenge in the fabrication process is the formation of the tunnel junction in between two antenna segments. As described above, for the tunneling mechanism to work well, the barrier thickness should not exceed a few nanometers [10]. Considering the upgrade in the tunneling due to the high localized electric field, we set our objective to creating a gap whose width is less than 5nm in between two conductor antenna segments.

Another important criterion that directly determines the response time of the device is the junction area. Unlike the second generation devices, in the third generation, the junction area is not directly dependent on the lithographic resolution. In our approach the junction area can be characterized by the sharpness of the bow-tie tip where the electrons tunnel into the other segment of the antenna. Our objective is to form the bow-tie as sharp as possible to satisfy the small junction area criteria of the antenna coupled CBC tunnel junction design.

Analogous to any antenna design, the geometry of the asymmetric bow-tie

antenna determines the abilities of the device. Thus, during the fabrication it is very important to keep the specified dimensions fixed which requires the minimization of the process variation. Particularly, to generate the resonance of the surface plasmons, the length of the antenna has to be an odd integer number of the half wavelength of the surface plasmons. Consequently, we set our objective to maintain the antenna segment dimensions constant while looking for the sharpest tip which forms the smallest gap at the tunnel junction by correcting the proximity effect, which is the main source of resolution limitations in EBL.

1.4   Outline

The remainder of this report is organized as follows: Chapter 2 starts with the background information on EBL and introduces the idea of Proximity Effect. It continues with mathematical restatement of PE and the classification of PE Correction techniques published so far. Chapter 2 ends by the presentation of the particular PEC technique based on linear programming optimization theory used in this thesis. Chapter 3 includes the details of experimental methods employed to fabricate the asymmetric bow-tie antenna. In Chapter 4, the results obtained are presented and the evaluation of these results are made.

Chapter 2

Background

2.1 Electron Beam Lithography

EBL is a commonly used tool in micro- and nano-fabrication processes requiring resolution of nanometric features. EBL employs very well focused, energetic (2-200KeV) electrons to transfer desired mask patterns to the target resist film which is usually an electron-sensitive material. Taking advantage of the very low quantum mechanical wavelength (pico meters) of high energy electrons, EBL does not suffer from the resolution limitations caused by diffraction as in the case of optical lithography. In addition, its high resolution key feature enables EBL to serve as a mask-less lithography technique, which makes it indispensable, especially for the research and development applications. On the other hand, EBL has several drawbacks that degrade its popularity in most industry based applications. First, EBL is a serial lithography technique, where the beam scans the pattern area pixel by pixel. This decreases the speed of the exposure and lowers throughput. Moreover, utilization of the electrons in EBL systems requires a high vacuum environment increasing the complexity of these systems together with their prices. Low throughput and expensive EBL units increase the cost of production, which is the most significant drawback of this technique.

Despite these drawbacks, the technique is capable of achieving the highest

feature resolution obtainable. The application area of EBL has been expanding everyday as the need for the fabrication of sub-micron structures increase owing to its proven success in high resolution lithography. EBL is frequently used for the fabrication of standard photolithography masks, where a thin chromium layer is patterned on glass. In this technique, the high cost and low speed of mask production is compensated by the recursive employment of very high quality photomasks for photolithography applications.

For our EBL applications, we used a RAITH e-line EBL unit, which is shown in figure 2.1 below.

Figure 2.1: RAITH e-line EBL unit

2.2 Electron Beam Proximity Effect

2.2.1 Introduction

Resolution is defined by different physical phenomenon in different lithographic processes. Unlike optical lithography, resolution in E-beam lithography is not limited by diffraction effects because the "effective" wavelength of the electrons is small compared to that of the photons used in optical lithography. Indeed, current EBL systems can focus the light into a less than 10 nm beam width on the substrate [42]. This beam diameter, or "spot size," is determined by the electron lens system used to form the beam. However, as soon as the highly focused electron beam enters the resist, electron interaction with the resist and the substrate causes undesired energy to be delivered to the points that are very distant from the incident beam point. This unwanted exposure in unintended regions of the resist is called "Proximity Effect", and determines the resolution limitations of e-beam lithography [5]. This effect usually creates the resolution limit of EBL tools.

2.2.2 Electron-Solid Interactions

Detailed characterization of electron behavior in the resist is crucial in e-beam lithography. The most important electron solid interaction that causes proximity effect is scattering. Today's e-beam lithography machines supply electrons that are in the energy range of 10-100 keV. Thus, electrons are highly energized when they hit the resist which allows them to penetrate through the resist and reach the substrate very easily. Two fundamental types of scattering occur during electrons travel in

the solid: forward scattering (b), backward scattering (a). [5] We deal with each of these in turn below.
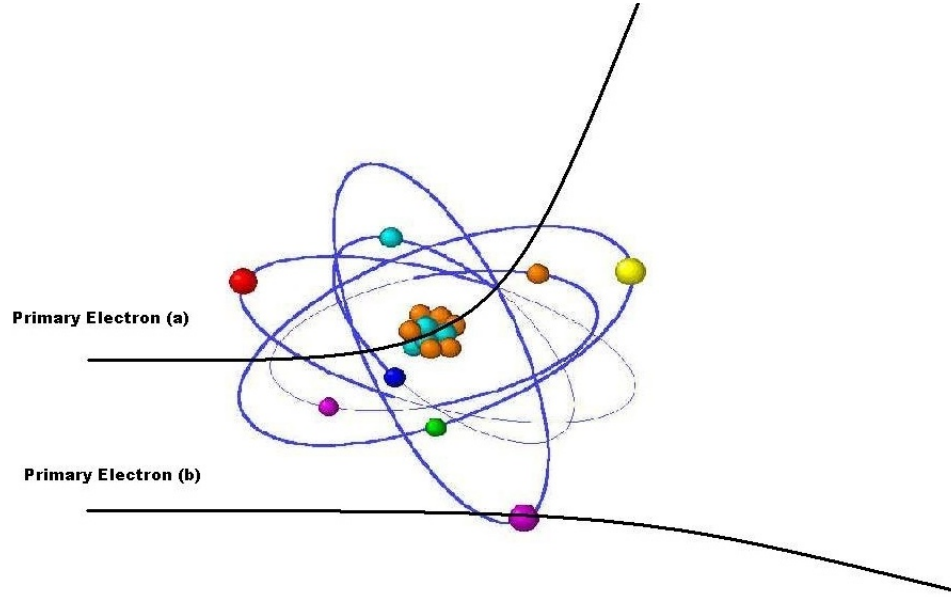
Figure 2.2: (a) Backward Scattering (b) Forward Scattering

2.2.2.1   Forward Scattering

Forward scattering is formed by the collision of primary electrons' traveling in the solid with the native electrons of the atoms that belong to resist or substrate molecules. Since it is highly probable for an electron to collide with another electron in the solid, forward scattering occurs frequently. This scattering is inelastic and causes a slight change in the trajectory of the electron as can be seen in figure 2.2 (a). Forward scattering contributes to broadening in the incident beam by either changing the trajectory of the incident electron or creating secondary electrons with a few eV of energy in the material.

2.2.2.2 Backward Scattering

Backward scattering happens occasionally when a primary electron hits a nucleus of the native atoms that belong to resist or substrate molecules. It is an elastic scattering process and the electron retains its energy but changes its direction as shown in figure 2.2 (b). Since the electrons continue to move with a high energy in a different direction, and they may even be returned to the surface at large scattering angles, they cause an energy transfer into the unintended areas in the resist. Although this happens very rarely, backward scattering causes a considerable effective broadening in the beam.

2.2.3 Exposure in EBL

Scattering events define the beam exposure area either by creating low energy secondary electrons (SE) through forward scattering or by changing the direction of the high energy primary electrons by backward scattering. Due to forward scattering primary electrons lose their energy and slow down on their way transferring their energy to secondary electrons. Moreover, high energy electrons change their direction after backward scattering and keep creating secondary electrons at a significant distance from the target beam point. Below, in figure 2.3, trace of an incident electron in the solid is shown.

Resist exposure happens when a chemical change occurs in the resist molecule chain. Low energy secondary electrons are the main source of exposure in the resist. They cause electron-electron interaction that leads to an energy transfer
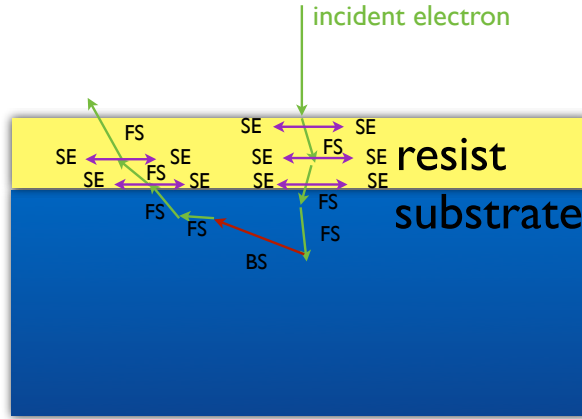
Figure 2.3: Electron behavior that cause the exposure in the resist

from electron to atom. As a result, this excess energy in the atom will either cause an excitation, where one of the electrons in the atom jumps into a higher energy state, or an ionization, where an electron leaves the atom creating a secondary electron in the material. If the electron being hit belongs to an atom in the resist, this collision will cause a chemical change in the resist molecule and result in the resist exposure.

2.2.4 Mathematical Modeling of Electron Beam in the Solid

Resolution improvement in e-beam lithography strongly depends on the understanding of proximity effect. In fact, computer simulations are proven to be the most accurate method of demonstrating proximity effect. Mathematical modeling of the e-beam in the solid can be stated as the first step of carrying this physical phenomena into the computer environment.

Energy density profile in the resist introduced by a point source of incident

electrons is often called Point Spread Function (PSF) and can be determined either by analytical or experimental methods. Analytical methods include the Monte Carlo Technique, where the path of electrons are predicted by the Rutherford scattering cross-section model and the energy deposition from incident electrons into the resist is calculated based on the Bethes continuous energy loss approximation. [44] Since the results of this method is obtained taking the average of individual electron behavior in the resist, its accuracy strictly depends on the number of electrons used during simulation. There are also several experimental techniques used to define PSF specific to a process, among which the doughnut method is the most popular [19] [36]. Although, these methods are good at predicting backward scattering parameters, they are not as reliable in forward scattering parameter determination, as its range is outside that of the imaging used to study such phenomena. The most general way to characterize the forward-scattering contributions to proximity effect is to develop a model of the whole energy deposition process and include the effects of the various scattering components as fitting variables. That is the approach taken here.

Mathematically, the simplest way of modeling PSF is superimposing two Gaussian distributions with different standard deviations, each representing the backward and forward scattered electrons as in equation 2.1 [5] [11].

$$f(r) = \frac{1}{\pi(1+\eta)}\left[\frac{exp(-\frac{r^2}{\alpha^2})}{\alpha^2} + \eta\frac{exp(-\frac{r^2}{\beta^2})}{\beta^2}\right] \tag{2.1}$$

The variables in the equation are as follows:

r-radial distance from the point of incidence

λ-half width of the electron distribution due to forward scattering

β-half width of the electron distribution due to forward scattering

η-ratio of backward to forward scattered electron distribution

Also, for some applications it is offered that adding an extra exponential data shows more accurate fitting. However, for our purposes two Gaussian PSF whose parameters are determined by Monte Carlo simulation technique is sufficiently accurate.

2.2.5   Physical Factors Affecting PSF

Both experimental and analytical results show that many variables contribute to proximity effect such as beam energy, substrate type, resist type, thickness, and development conditions.

2.2.5.1   Beam Accelerating Voltage

Beam energy has a major effect on the energy distribution profile in the resist and substrate. As the energy of the incident beam increases, the speed of the electrons traveling in the resist increase, while energy deposition per unit path length decrease. Thus, electrons dissipate their energies in a very short vertical range $(1.5\mu m)$ and spread laterally due to forward and back scattering, as well as secondary electron generation. On the other hand, electrons in a very high energy beam ($\geq$ 50KeV) may reach the substrate without generating enough secondary

electrons during their travel in the resist. Moreover, these high energy electrons experience plenty of backward scattering in the substrate and give rise to an excessive lateral broadening of the energy deposition range. In conclusion, forward scattering dominates in the low energy beams, defining a very short ($\leq 2\mu m$) forward scattering range; on the other hand, with the high energy beams backward scattering dominates, resulting in a large lateral scattering range ($\geq 2\mu m$). Below, in figure 2.4, this phenomena is demonstrated (the images were generated by Monte Carlo Simulation). In this figure the first row shows the electron trajectories in both the resist and the substrate. It can be observed from the figure that the electron-substrate interaction increase as the energy of the electrons increase, triggering backward scattering events. In the second row of the figure only the resist is shown. These plots show that at low acceleration voltages, although the short range resolution is bad, in the long range there is no proximity effect. However, for the high acceleration voltage case, the resolution is extremely good in the short range, but the backward scattering carries the energy further and the long range exposure interference is high [44].

2.2.5.2   Substrate Material

The PSF has a substrate material type and thickness dependence. Probability of backward scattering occurrence is higher in large atomic number (Z) substrate materials due to the relatively larger nucleus in their atoms. In addition, the thickness of the high-Z material affect the backward scattering frequency.
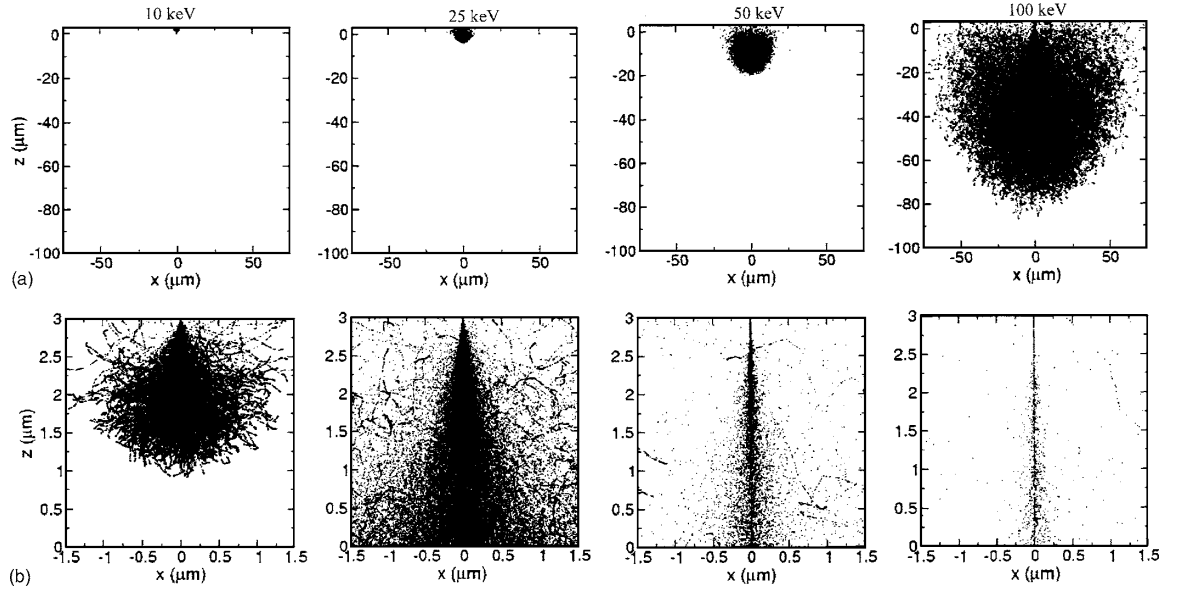
Figure 2.4: Secondary electron distribution (a) in both the resist and substrate (b) within the resist at different beam energies

2.2.5.3 Resist Material and Thickness

Resist film parameters also determine PSF characteristics. First, in thick resist films, the beam has more space to broaden and this creates a dose accumulation at the bottom of the resist. Moreover, each resist type is exposed through a different chemical reaction sequence. Thus, the same energy deposition can result in different exposure profiles according to the resist used.

2.2.5.4 Chemical Development Conditions

Every developer shows a different development profile. Moreover for each developer it is expected to see different results depending on the developing time or temperature. Thus, even if all the parameters defining PSF are kept the same,

different development conditions will result in different beam profiles in the resist.

2.2.6 Proximity Effects in Implementation

In practice, two main types of proximity effects are observed: (1) Intra-shape proximity effects, and (2) Inter-shape proximity effects [28]. These are shown in the figure below and described in the next sections.
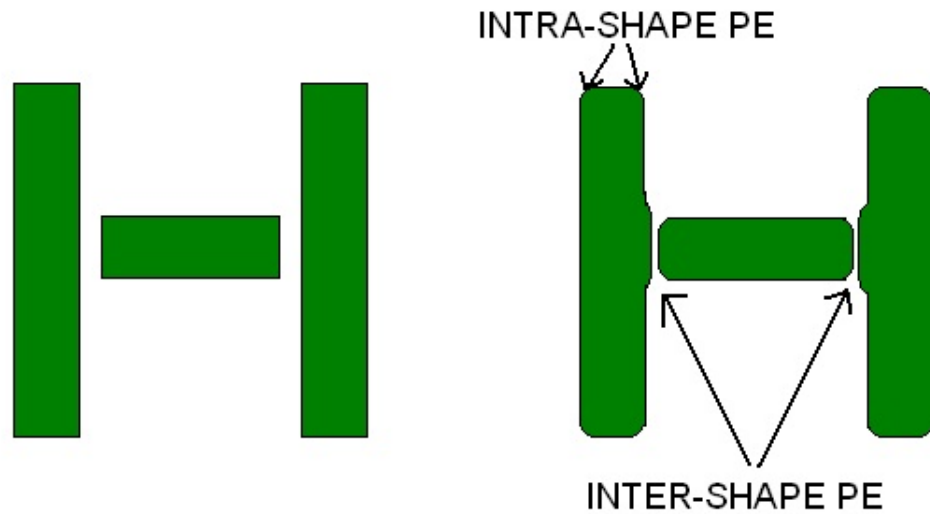
Figure 2.5: Inter and Intra proximity effects in implementation

2.2.6.1 Inter-Shape Proximity Effects

Inter-shape proximity effects are introduced by the long range backward scattering of the electrons. Backscattered electrons cause exposures away from the incident beam and contribute to the overexposure of the adjacent patterns as shown in figure 2.5.

In practice inter-shape proximity effects lead to a common phenomena called critical dimension (CD) variation. Specifically, if two identical patterns, one in a densely packed area and the other in a sparsely packed area are exposed identically, the first one will end up with larger dimensions than the second. In figure 2.6 this problem is demonstrated.
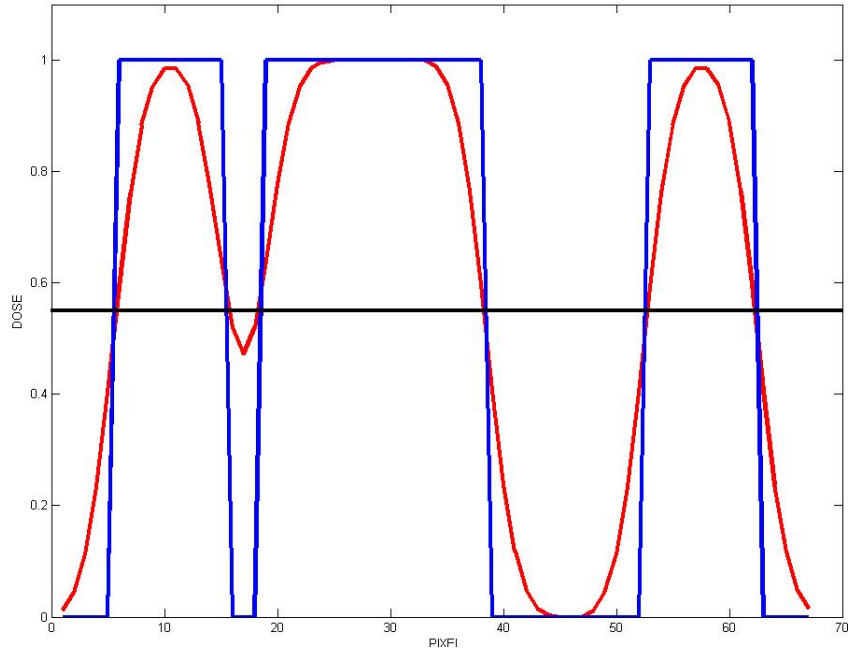
Figure 2.6: Critical Dimension variation

2.2.6.2 Intra-Shape Proximity Effects

Intra-shape proximity effects are introduced by the short range forward scattering of the electrons. Due to the accumulation of the forward scattered electrons a non-uniformity occurs inside the pattern element. This phenomena has two types of outcomes: pattern size dependent exposure, and deterioration in shape fidelity.

a) Pattern Size Dependent Exposure

Dose accumulation shows different profiles depending on the dimensions of the isolated structures. That is, when different sized, isolated patterns are exposed identically, the smaller patterns get less exposure than the bigger ones. This phenomena is demonstrated in figure 2.7 below.
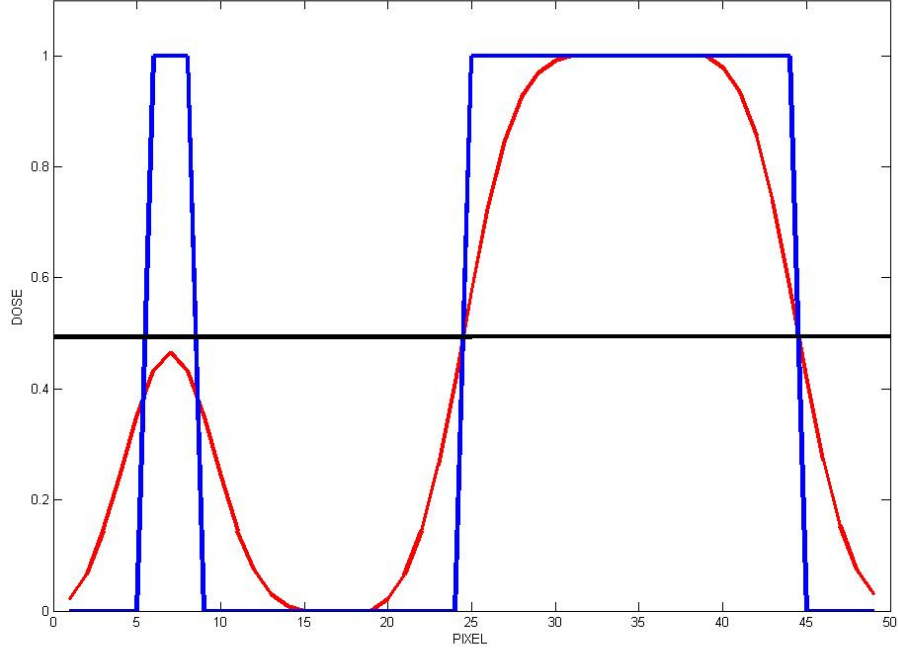
Figure 2.7: Pattern size dependent exposure

b) Deterioration in Shape Fidelity

Deterioration in shape fidelity is another consequence of "Intra-Shape Proximity Effects". As shown in figure 2.7, dose accumulation varies in the pattern according to pixel placement. This results in two types of deterioration in the pattern shape: corner sharpness, and line edge roughness. Since the pixels at the corners are not surrounded by neighboring pixels, which contribute to the dose accumulation, corner pixels are usually left unexposed, which results in rounded corners. Also,

dose variation at the edge pixels results in an undesired roughness at the borders of the pattern.

2.3   Mathematical Statement of Proximity Effect Problem

Mathematical modeling of the PE plays a crucial role in the development of correction algorithms. The mathematical statement of PE can most accurately be done by modeling the physical parameters as functions, where the variables address the location on the 2D pattern. Below is the terminology to be used in modeling [41].

$G(x, y)$: Point Spread function (described in the text).

$M(i, j)$: Interaction matrix. This function captures the degree to which

         energy deposited in the ith pixel contributes to energy absorbed in

         the jth pixel. It is derived from the point spread function.

$P(x, y)$: Target pattern dose distribution function. This is the desired dose distribution.

d_p : Target pattern dose distribution vector. A 1-dimensional vector whose entries

         can be viewed as a discretization and "unstringing" of

         the target pattern function.

$D_I(x, y)$: Incident dose function. This gives the amount of energy directly deposited by

         the beam in a given pixel, indexed (i,j).

d_I : Incident dose vector. A 1-dimensional vector whose entries

         can be viewed as a discretization and "unstringing" of

         the incident dose function.

$D_A(x, y)$: Absorbed dose function. This gives the total energy actually absorbed

         by a given pixel, indexed (i,j).

d_A : Absorbed dose vector. A 1-dimensional vector whose entries

         can be viewed as a discretization and "unstringing" of

         the absorbed dose function.

(i, j) : Discretized pixel address.

     Note that all of the continuous two dimensional distribution functions can be discretized by replacing the (x, y) by the index (i, j). The continuous and the discrete absorbed energy profile can best be approximated by the convolution of

the point spread function and the applied dose matrix as in equations 2.2 and 2.3, respectively.

$$D_A(x, y) = G(x, y) \otimes D_I(x, y) \tag{2.2}$$

$$D_A(i, j) = \sum_{k=-\infty}^{+\infty} \sum_{l=-\infty}^{+\infty} G(i, j) D_I(i - k, j - l) \tag{2.3}$$

"Ideal exposure" happens when D_A is equal to P, also defined as below:

if $P(x, y) = 1$, then $D_A(x, y) = 1$

or if $P(x, y) = 0$, then $D_A(x, y) = 0$

In a mathematical sense, proximity effect arises simply because the ideal exposure defined above is not possible by applying a uniform dose to the target pattern. That is, the difference between $D_A(x,y)$ and $P(x,y)$ increases as $G(x,y)$ degrades from being a delta function to a Gaussian distribution. Various proximity effect correction methods have been developed until today and they fundamentally aim to meet the ideal exposure condition. The first group of PEC methods deals with the incident dose matrix (D_I) modification either by varying the dose per each pixel in the pattern matrix (dose modulation techniques) or by altering the pattern matrix but keeping the dose same everywhere (shape modulation techniques). The second group basically intends to modify the point spread function (G) (physical modification techniques) so that it converges to a delta function.

2.4   Classifying PEC Methods

2.4.1   Physical Modification Techniques

A very straightforward way of alleviating the negative aspects of proximity effect is to decrease the range of point spread function. Physical approaches such as using high beam energies, low beam energies, and multilayer resists all intend to modify the point spread function in various ways. Although physical modification techniques seem very simple and practical, they are usually very application specific and do not offer a generic solution to the proximity effect problem [22, 23, 26, 33, 35].

2.4.1.1   High Beam Energies

As described in section 2.2.5.1, as the beam energy increases, the range of forward scattering in resist decreases. In addition, electrons with high energy are able to penetrate deep into the substrate, which almost eliminates the backward scattering effects in the short range. Although these two factors listed above increase the resolution, using high energy beam introduces significant drawbacks to EBL. High energy beam electrons experience backward scattering and these back scattered electrons create a large effective beam broadening. Moreover, due to the low secondary electron generation rate in the high energy beam, throughput is low compared to the low energy beams. In summary, short range proximity effects can be lessened using high energy beams. In turn, this causes worsening in the long range proximity effects, damage in the substrate and low throughput [23, 26, 35].

27

2.4.1.2 Low Beam Energies

Another method of decreasing proximity effects is to employ low energy beams. When the incident beam energy is relatively low, electrons deposit most of their energy into the resist causing a lateral expansion in the exposed resist area. Although this seems like a negative property, since the electrons have less energy when they reach the substrate the backward scattering is considerably reduced. Thus, low energy beam exposure significantly annihilates the long range proximity effects. Furthermore, low energy beam increases the throughput due to the efficient energy deposition onto the resist. On the other hand, penetration depth is much shorter, and this inhibits the thick resist applications using this method [23, 26, 33] .

2.4.1.3 Multilayer Resist

Multilayer resist application has been offered to reduce the long range proximity effects by diminishing the backscattering of electrons. This method employs a very thick $(2-3\mu m)$ polymer layer below a very thin actual resist layer. Although this polymer layer is not sensitive to electrons and it does not play an active role in real image forming, it cushions the high velocity electrons before they reach the substrate and lessens backscattering. However, this method is not very practical due to its high complexity in the fabrication process [22, 26].

2.4.2   Shape Modification Techniques

Shape Modulation is a very rarely used PEC method for direct write EBL, however it is very convenient for e-beam projection lithography, where the option of dose modulation within the mask pattern does not exist. This method intends to correct the dose profile of a feature by remodeling and/or changing the dimensions of the original pattern.

One of the first shape modulation techniques was proposed by Parikh [29]. This technique suggests to change the design dimensions of shapes. This requires solving a set of non-linear equations in order to find the modified dimensions, which prevents this method from being used for realistic applications due to the complexity in computation. Also another similar approach was addressed by Sewell [37], where the look-up tables are employed instead of equation set computation for the basic shapes required for mask fabrication.

Another recently addressed technique for pattern shape modification exploits the area density map for the determination of the modified pattern sizes [25]. In this algorithm, the area density map is designated based on the backscattering energy accumulation. This fact constrains this method to the very high energy beam EBL applications where the forward scattering effect is negligible.

2.4.3   Dose Modification Techniques

The Dose Modification (DM) Technique for PEC is the most frequently studied and implemented technique, owing to its simple approach to the problem: a linear

system with clearly defined variables. In this approach the unknown variable is taken as the incident dose matrix (D_I) where the PSF (G) and the target pattern matrices (P) are predetermined inputs of the system. As in all other PEC methods, the fundamental goal is to satisfy the ideal exposure. In other words, solving for the input dose matrix by employing various computational methods in order to associate the absorbed dose matrix (D_A) to the target pattern matrix (P) constitutes the basics of this approach.

Dose modification techniques developed so far can be analyzed under three main groups: linear methods, nonlinear methods and edge slope modification methods [16]. The salient features of each are summarized below.

(a) Linear Methods   (b) Non-Linear Methods   (c) Edge-Slope Modification Methods
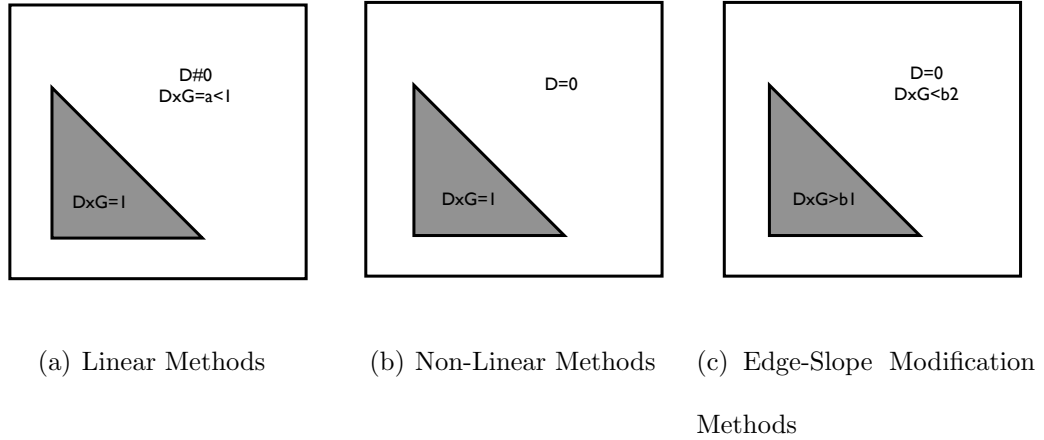
Figure 2.8: Dose Modification Methods

2.4.3.1 Linear Methods(LM)

Linear dose modulation methods constrain the absorbed energy to be uniformly equal to some "nominal" dose (sometimes called the unity dose, or dose-one) inside the target pattern area, and less than a certain number (an effective "dose-

zero" outside the pattern area. In addition, this approach does not require the applied dose to be zero in the pixels comprising the unwritten field of the target pattern matrix. The summary of the linear methods is shown in figure 2.8 a) and the general equations needed to be solved by the linear methods are given in equation 2.4.

$$D_A \equiv P \Rightarrow P = G \otimes D_I \Rightarrow D_I = G^{-1} \otimes P \qquad (2.4)$$

The first and the most primitive LM, exact dose correction, was proposed by Kern [20]. It is called exact dose correction because this method leads to a solution using deconvolution techniques that strictly satisfies the ideal exposure where the pattern matrix (P) equals the absorbed dose matrix (D_A). The process sequence of this method is summarized in the flow diagram shown in figure 2.9. One of the drawbacks of this tactic is that if the input dose in the off-pattern pixels are assumed to be zero, this algorithm generates negative input dose values, which is impractical in real life applications. This obstacle was overcome by offsetting the pattern matrix (P) by a proper amount in some applications. Furthermore, since this technique uses a pixel-by-pixel deconvolution, it is computationally impractical.

The second LM was presented by Owen et.al. under the name of GHOST [27]. This method requires the exposure of the off-pattern areas in order to compensate the inhomogeneous background dose generated by the backscattered electrons. GHOST performs the same basic function as Kern's method, but it doesn't require long computations. Nevertheless, exposing both the pattern and off-pattern pix-
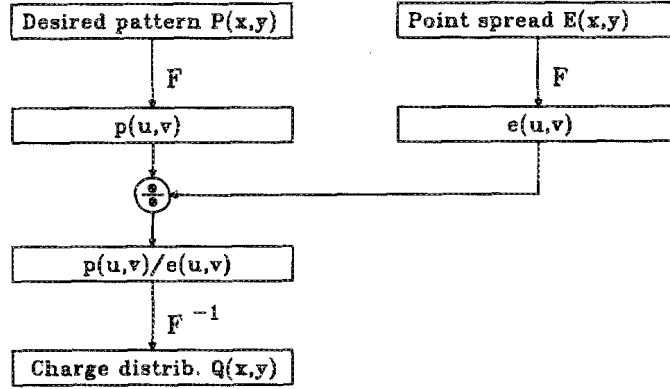
Figure 2.9: Exact Dose Correction Algorithm by Kern

els, i.e. the whole wafer, is the major disadvantage of this approach because it is unnecessarily time consuming.

In addition, Crandall mathematically demonstrated that GHOST can be analyzed under Newton Inverse techniques, where the inverse Fourier Transform of the PSF matrix (G) can be approximated by a Newton iteration method [6]. However, this mathematical approach revealed that any degree of Newton inverse prosecution, including the first degree, GHOST, provides an improvement in the minimum feature size while exacerbating the contrast, hence unveiling another drawback of the GHOST method. Peckerar, et. al[1] have shown that there are certain important cases for which GHOST simply fails. These are cases in which the small, highly resolved features are surrounded by much larger patterns. As a general strategy for economically achieving high resolution is to write the course features with a larger beam and to surround the fine features with those written with the broad, low resolution beam, the GHOST method has serious drawbacks.

Another LM utilizing deconvolution was suggested by Eisenmann et al. with

the name PROXECCO [8]. This method differs from the other deconvolution methods by using an inverse filter to remove the high frequency components of the Fourier transformed PSF function. This allows the correction to be done with larger pixels and thus reducing the computational requirements of the deconvolution process. However, eliminating the high frequency components deteriorates the precision of the correction. Also, for very large patterns, simply increasing the pixel size only doesn't make this method computationally efficient.

2.4.3.2 Nonlinear Methods

Nonlinear methods (NLM) forces the absorbed energy on the intended pattern pixels to be one as in the LM, however they do not have any restriction on the accumulated energy on the off-pattern pixels. Hence, this strategy decreases the number of unknowns from the entire pattern matrix elements to the simply intended shape elements because the dose matrix elements outside the patterned area are preset to 0. This technique is summarized in figure 2.8 b).

The first NLM, "Self Consistent Dose Correction" was proposed by Parikh [28]. This method aims to fix the total absorbed energy on the intended pattern area by solving a significant number of linear equations to determine the amount of dose necessary per predefined pixel, yet taking no notice of the exposure on the off-pattern areas. The first handicap of this method stems from the accumulated dose in the off-pattern areas. The exposure in the neighboring pixels of the pattern decreases the contrast at the edges, thus this degrades the CD linearity. In addition,

solving a linear system with such a large number of equations is impractical.

Pavkovich also came up with an approximate solution, which can be analyzed under nonlinear methods [30]. In this technique after the pattern is segmented into pixels an average dose is approximated by a formula. This formula is derived from the basic resultant exposure equation given in equation 2.4 by disregarding the exposure on the off-pattern pixels and targeting at a uniform exposure inside the pattern. In addition to the negative aspects of a typical nonlinear method, this technique ignores the forward scattering affects and only works toward correcting the backscattering PE problem.

2.4.3.3   Edge Slope Modification Methods

On deeper analysis of the PE problem, the value of increasing the contrast at the pattern edges becomes evident. This idea was first introduced by Veneklasen et. al. with the words: "Thus the goal of proximity correction is to expose all the pattern edges isofocally with maximum exposure contrast." [39]. Here, the word isofocal signifies the exposure dose at the edge of a feature when a uniform dose profile is applied and the PSF is taken to be a symmetric Gaussian as in equation 2.1. It is always equal to half of the applied dose under the specified conditions as shown in figure 2.10. Also, it is obvious from this figure that as the PSF expands the slope at the edge of the dose profile degrades.

Subsequent to setting the new goals of PEC, Veneklasen et. al. presented a new algorithm for PEC [39]. In this technique, long range and short range correction

(a) Uniform dose profile

(b) PSF with different alpha parameters

(c) Accumulated dose, or the convolution of the square and various gaussian
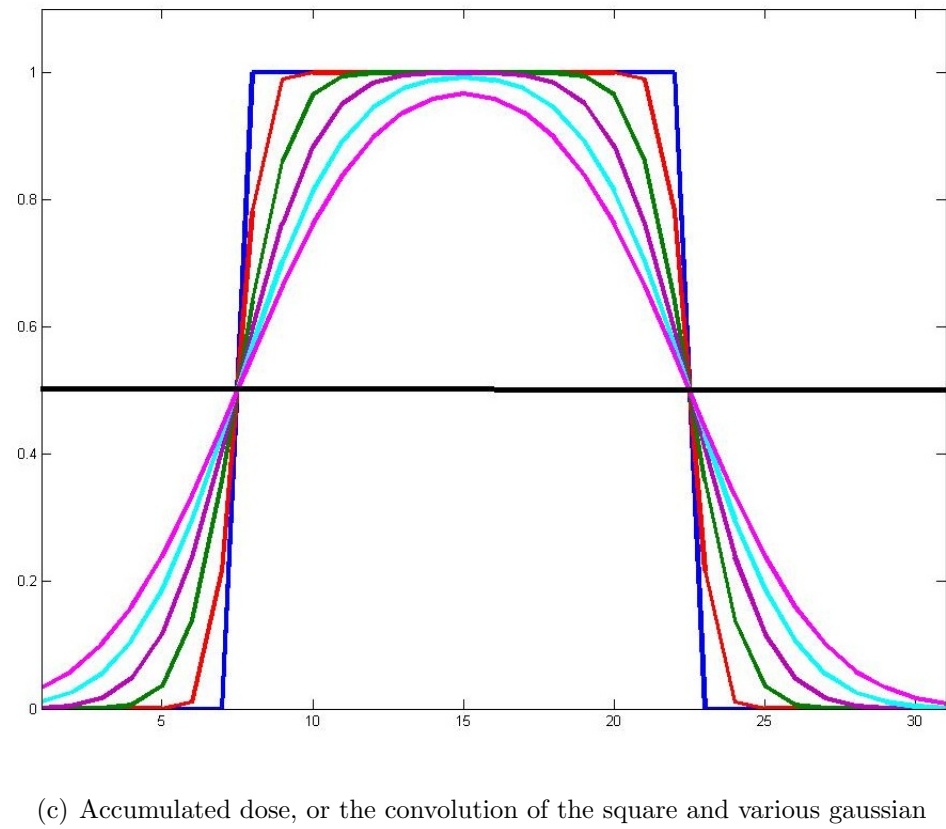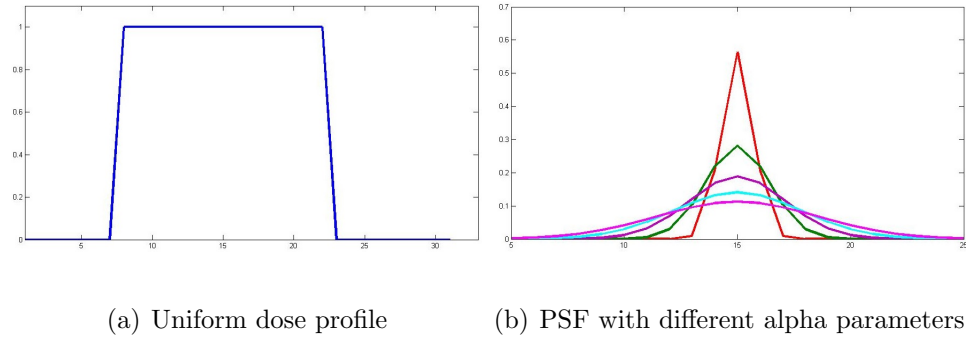
Figure 2.10: Various edge contrasts depending on the PSF parameters

algorithms are defined independently. The long range correction algorithm targets at fixing the edge dose of all the features to isofocal exposure threshold through a recursive method and the short range correction algorithm focuses on increasing the contrast at the edges of the features by biasing the dose applied to the whole feature only on the border pixels. Since this algorithm considers the short range effects only as an intra feature problem on the basis that the closest neighbor feature is not in the range of forward scattering, this method is not applicable to the nano-patterning applications where the gap between the features need to be comparable to the short range PE.

2.5   PEC by Dose Modulation Using Linear Optimization Theory

In the evolution of the PEC techniques by dose modulation, many different approaches have been presented. We can analyze these as three different groups (Linear Methods, Nonlinear Methods, and Edge Equalization Methods). Although most of these methods have proven their success, they all suffer from various draw-backs, which limit their usage to specific applications. For instance, linear methods put too many restrictions on the absorbed energy by equating the exposure in both the on- and off-feature pixels. Thus, this method either requires extensive math-ematical computations to solve for each dose pixels or redundant exposure of the whole wafer to satisfy the strict constraints. Subsequently, nonlinear methods are introduced to relax the nonessential limitations of the linear methods by only defin-ing constrains on the feature pixels. However, since this method completely ignores

the accumulation in the neighboring pixels of the feature, it creates very low contrast in the absorbed energy at the borders of the features. Hence, nonlinear methods cannot correct the PE related problems, since most of these problems stem from low contrast at the edges. Eventually, with the invention of edge equalization methods, the mathematically unsound PE problem was corrected and the goal of the PEC methods was changed from strict fulfillment of the ideal exposure condition to satisfying a certain contrast level at the margins by assuring a threshold exposure on the borders of the feature. Some techniques were offered under this category, but they remained pattern particular. However, restating the PE as a linear optimization problem introduced the most inclusive, easy to implement, realistic, general, pattern- and physical circumstance-independent PEC technique enabling the utilization of the linear programming (LP) methods.

2.5.1 Brief History of Linear Optimization in PEC

The application of LP methods to the dose modulation problem of PEC was first proposed by Carroll [4]. Although the adaptation of PE as a LP problem was precisely done and the solution to the LP problem was successfully offered as a Simplex approach by Carroll for one dimensional systems, the capacity of the computers in 1980's did not allow this method to be employed for practical large database applications. The second attempt to use LP for the solution of dose modification problem was made by Peckerar et. al., where Carroll's method was extended to be used in two dimensional and larger systems [31]. Peckerar not only

took the advantage of more sophisticated computer system architectures, but also offered the implementation of parallel computation to speed up this LP process for real world applications. In addition, he upgraded the previously offered simplex method with interior points method, seeing the progressive improvements in LP in the last decade [32].

2.5.2 Mathematical Redefinition of the PE problem

The observation of the proximity effects can best be done by computing the total accumulated dose per each pixel. As described earlier, this accumulation can be calculated by the convolution of the incident dose matrix with an "interaction matrix" generated from the PSF . This convolution can also be carried out by a simple vector multiplication shown in equation 2.5. In the equation, d_I represents the input dose vector[1] and d_A symbolizes the total accumulated dose vector. The matrix M is called the "interaction matrix" and it is obtained from the PSF. In the matrix M, elements of a particular row represents the ratio of the dose accumulated in each pixel of the pattern due to the exposure in a single pixel corresponding to the row. Hence, addition of elements in a row should give one for a normalized PSF.

$$\mathbf{M} * \mathbf{d_I} = \mathbf{d_A} \tag{2.5}$$

As discussed, early linear approaches attempted to achieve $(\mathbf{D_A} \equiv \mathbf{P}.)$ This led to mathematical inconsistencies (negative dose requests.) The mathematical

---

[1]This is a 1-dimensional vector whose entries record the beam-applied energy dose to each individual pixel.

model used for the linear optimization approach is relatively different compared to earlier approaches. First of all, it recognizes that the $D_A \equiv P$ requirement is unrealistic and may be mathematically "infeasible". Second, it does not demand a single dose in the exposed field and zero dose in the unexposed field. But rather, the demand is for the exposed pixels to achieve a dose greater than some exposure dose and the dose to the unexposed field should be less than a tolerable level. We summarize the Linear Optimization Approach as follows:

$$f = \|\mathbf{M} * \mathbf{d_I} - \mathbf{d_p}\| \rightarrow minimum \tag{2.6}$$

Other Approaches:

$$f = \|\mathbf{M} * \mathbf{d_I} - \mathbf{d_p}\| = 0 \tag{2.7}$$

The linear optimization approach aims to find the extrema (minimum or maximum) of a given function under certain constraints. In order to apply techniques offered by linear optimization theory to the dose modification line of PEC, it is essential to remodel the PE problem as shown next [31].

The approach taken from [31] is to develop a physics-based optimization criteria and express these as a "cost function". One such cost function is minimizing the total dose applied, as expressed in equation 2.8

$$c(d_I) = \mathbf{d_p^T} * \mathbf{d_I} \tag{2.8}$$

The constraints to be satisfied by the variable of the cost function are listed below:

$$\mathbf{d_{Ae}} \geq \mathbf{b_1} \tag{2.9}$$

$$\mathbf{d_{Au} \leq b_2} \tag{2.10}$$

$$\mathbf{d_I \geq 0} \tag{2.11}$$

where d_{Ae} is the dose to an intentionally exposed pixel and d_{Au} is the dose to a pixel in the unexposed field.

The mathematical model stated by the equations 2.9 -2.11 above is solvable for the entries of the vector d_I, using linear optimization methods such as simplex or interior point methods. Indeed, the basic mechanism used by these methods can be summarized like this. The constraint equations form planes in the n-dimensional space where n is the number of pixels in our case. And these planes intersect with each other forming a geometrical structure called simplex. Another plane in the same space represents the cost function. In order to find the minimum of this function, the cost function plane is lowered until it intersects with only a single point of the simplex. It is mathematically proven that if a solution exists for a particular problem, it has to be on one of the vertex points of the simplex. As a result, the coordinates of the vertex point where the cost function plane touches the simplex gives the solution (the incident dose matrix in our case).

The first constraint in equation 2.9 is defined for the feature pixels so that total dose they obtain is over a certain threshold, $b1$. This threshold is a property of the resist system (type, thickness of the resist) being used and can be stated as the minimum dose to expose one pixel completely.

The second condition expressed in equation 2.10 is for the off-feature pixels, where no direct exposure is sent. These pixels are required to have a total dose

below a certain threshold, $b2$ so that they are not exposed.

The third constraint in equation 2.11 is a natural outcome of using linear optimization theory to solve this problem, because it requires all optimized variables to be positive. This is a great advantage of working with this technique because negative dose values will never be part of a true solution.

It is important to mention that the mathematical model introduced above takes the real world resist parameters into consideration. The thresholds used in equations 2.9 and 2.10 can be associated with the D_1 and D_0 dose values shown in the resist contrast curve in figure 2.11. In addition, these two parameters define the edge contrast in correlation with equation 2.12. Although the fundamental objective of PEC is to solve this mathematical system so that the edge contrast defined in equation 2.12 is maximum, nature might not always permit the solution of this system with the desired thresholds. This information is precious because it designates the limits of the e-beam lithography for a distinct pattern. When this technique tells us that solution is not feasible, one has to relax the thresholds by sacrificing the high contrast. Despite the fact that this will induce incrementally more proximity effect, one can still get satisfactory results.

$$C_f = \frac{D_A(boundary) - D_A(boundary + 1)}{D_A(boundary) + D_A(boundary + 1)} \tag{2.12}$$
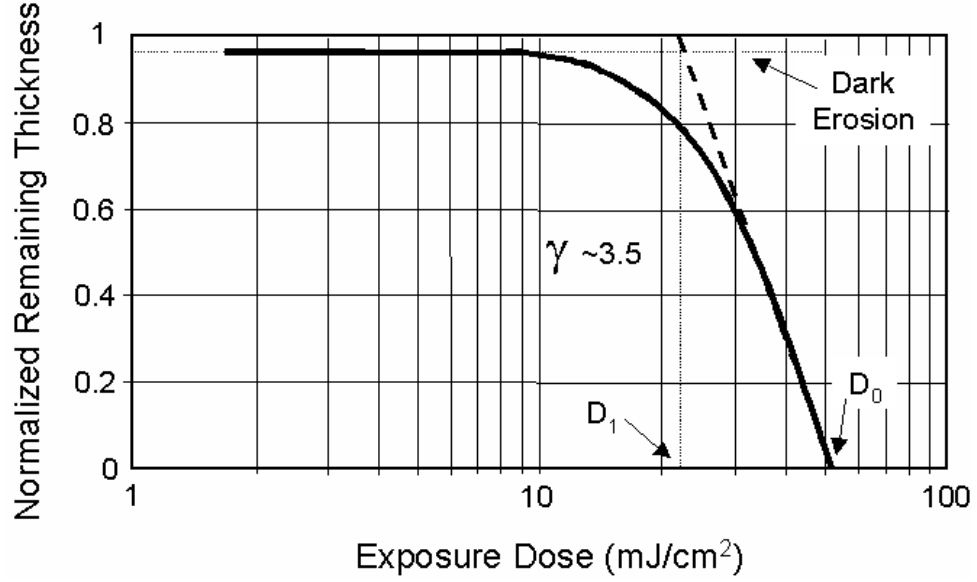
Figure 2.11: Resist Contrast Curve

2.5.3 Implementation of the PEC Using Linear Optimization Theory

Linear optimization theory is applied to the dose modulation problem of PEC. The mathematical model derived for the solution of the proximity problem is a typical issue for linear programming and can be implemented using basic linear programming methods like Simplex or Interior Points Methods. Due to its relatively higher speed, interior points method is preferred for this application [32].

The algorithm shown in figure 2.12 was used. The software takes four main groups of inputs. The first input is the target pattern matrix where two values are used in the matrix elements to define the structures. Linear programming parameters form the second input group, this data is used to regulate the edge contrast and define an interval for the solution. The third input is a matrix representing the PSF. Finally, the last input group carries the information of the size of the partitions and the buffer around these partitions. Some minor modifications, namely

segmentation, and the formation of the M matrix are executed on the inputs so that the data format is ready to be processed. The LP solver, which uses interior point methods, is run for each partition of the pattern individually. Performing the LP process in partitions instead of at once is offered by Peckerar et. al. in view of the fact that partitioning decreases the computation complexity and increases the time efficiency of the process. In addition, it enables the utilization of parallel processing which is another way of decreasing the process time. Each partition execution yields a flag informing the user of the performance of the operation. A "-2" means that solution is not possible under the given conditions. The code stops running and asks the user to go back and change the input parameters. However, a flag equal to "1" reveals that the operation is performed successfully and the results are valid. If valid results are obtained for every partition of the pattern, these are gathered all together and the universal input dose matrix is obtained. Convolution of this matrix with the PSF matrix gives the expected total accumulated dose values on each pixel. For the purpose of comparison, a uniform dose profile is also convolved with PSF matrix to find the total accumulated dose profile if no PEC is applied.

2.5.4 Linear Optimization and Shot Noise Minimization

Relying on the increase in the edge slope of the accumulated dose as an outcome of the PEC technique explained above, we claim that the disturbances created by the dose fluctuations (shot noise in the applied dose) can be ameliorated in the course of eliminating PE. Throughout our previous calculations, dose per pixel is

always taken as a fixed number. In EBL, commonly used parameter dose stands for the amount of charge per area and can also be stated in terms of the number of electrons hitting on the surface or the beam current. This concept is summarized below in equation 2.13. As opposed to our previous assumptions, where the dose is taken as constant in a pixel, there is a shot noise disturbance in the number of electrons arriving at a particular pixel. In other words, the number of electrons we are planning to send into a specific pixel is only an average number of electrons that arrive on the pixels that are supposed to have the same dose. Indeed, the actual number of electrons entering a pixel is more than, equal to or less than the intended value due to statistical fluctuations. These statistical fluctuations occur as a result of discretely charged particles movement that forms the current. This physical phenomena is called "Shot Noise".

$$D = N * e = J * T * A \qquad (2.13)$$

D: Dose($Coulomb/Pixel$)

N: Average number of electrons hitting on a single pixel

e: Elementary charge($Coulomb$)

J: Current Density($Coulomb/Seconds * cm^2$)

T: Exposure time($Seconds$)

A: Pixel area($cm^2/pixel$)

The number of electrons arriving at a single pixel can be modeled as a Poisson random variable. Hence, in accordance with the Poisson distribution given in equation 2.14, the standard deviation from the average number of electrons can be stated as in equation 2.15.

$$f(k; N) = \frac{N^k * e^{-N}}{k!} \tag{2.14}$$

$$\sigma = \sqrt{N} \tag{2.15}$$

k : Number of occurrences of an event (the probability of which is given by the function)

N: Positive real number (equal to the expected number of occurrences that occur during the given interval)

Based on this theory, we modified our simulations so that the consequences of these statistical fluctuations can be observed and the improvements provided by the PEC method is proven. In figure 2.13 our revision in the algorithm is summarized. For this modification, first a considerable number of dose values with probabilities defined by the Poisson distribution whose mean is entered as the initial dose associated with that pixel are generated. Then, a random number is generated with a uniform distribution in order to select one of these numbers to determine the new dose value. Principally, the dose value of each pixel is modified taking the shot noise contribution into account. Next, using these adapted dose matrices new total accumulated dose matrices are formed.
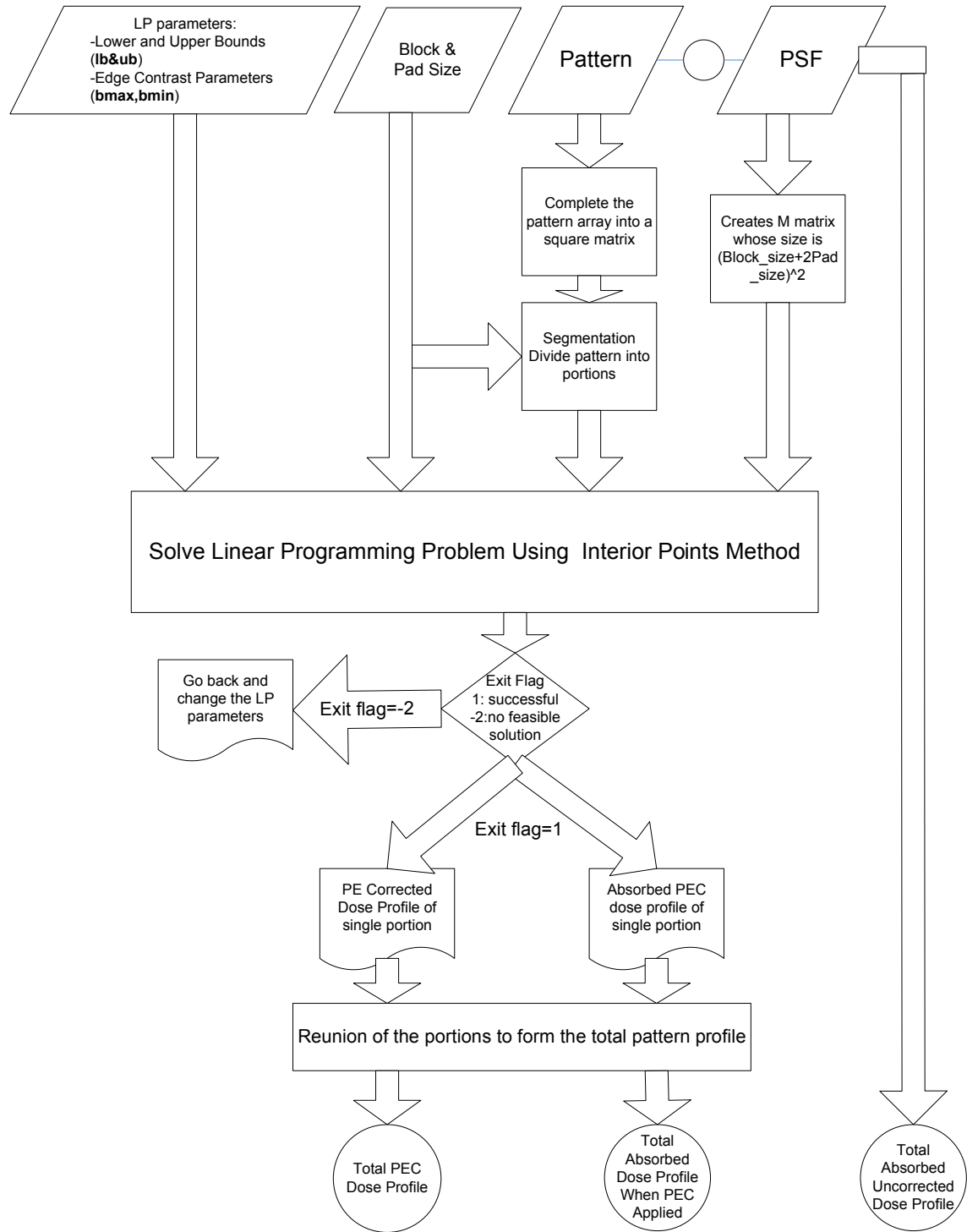
PROXIMITY EFFECT CORRECTION ALGORITHM

LP parameters:
-Lower and Upper Bounds
(**lb&ub**)
-Edge Contrast Parameters
(**bmax,bmin**)

Block &
Pad Size

Pattern

PSF

Complete the pattern array into a square matrix

Creates M matrix whose size is (Block_size+2Pad_size)^2

Segmentation Divide pattern into portions

Solve Linear Programming Problem Using Interior Points Method

Go back and change the LP parameters

Exit flag=-2

Exit Flag
1: successful
-2:no feasible solution

Exit flag=1

PE Corrected Dose Profile of single portion

Absorbed PEC dose profile of single portion

Reunion of the portions to form the total pattern profile

Total PEC Dose Profile

Total Absorbed Dose Profile When PEC Applied

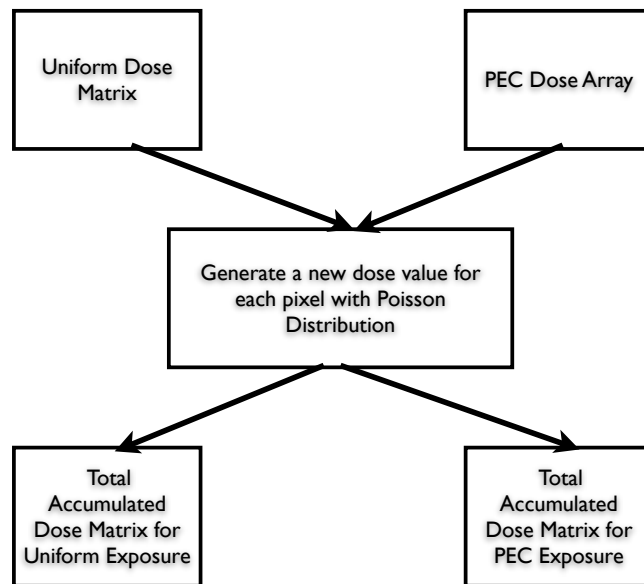Total Absorbed Uncorrected Dose Profile

Figure 2.12: PEC Algorithm

Figure 2.13: Shot noise minimization incorporated into the PEC algorithm

Chapter 3

Experimental Methods

3.1 Introduction

For the implementation of PEC, two main types of process flows were followed. Working with different types of resists for EBL during the patterning stage created the main difference between these two processes. The first method uses Polymethyl-Methacrylate (PMMA), which is the most common positive tone electron resist; while the second process uses Hydrogen-Silsesquioxane (HSQ), a negative tone electron resist. In this section, characteristics of these two e-beam resist systems will be presented and the fabrication sequences will be described in detail.

3.2 EBL Resists

Lithography is a technique whereby patterns are created on a substrate. In EBL an electron beam "writes" the pattern, pixel-by-pixel, into a radiation sensitive material. E-beam resists act as the radiation sensitive pattern transfer medium. In other words, e-beam resists partially change their chemical composition in the regions where the electron beam hits with a very high resolution; as a result of this, the intended pattern forms as a molecular the uniformity in the coated resist layer. The change in the chemical characteristics of the e-beam resists occur in two fundamental

ways depending on the type of the resist used, namely positive and negative resists. In the case of PMMA (a positive resist), e-beam exposure disturbs the molecule chains by breaking them into smaller fragments; as a result, these regions become less stable and more soluble in the developing solution. After developing, the already exposed parts of the positive resist layer are removed creating vacancies in the intended pattern, which allows the application of additive fabrication methods and lift of process. On the other hand, negative tone resist develop a more sturdy phase due to the cross-linking in the molecular stage in the exposed regions, this leads to a less soluble molecular structures in the exposed regions. After developing, everything but the exposed pattern areas are dissolved in the developer solution. This resist system allows the subtractive fabrication processes such as etching. In the sections below the characteristics of the positive and the negative resists used in our fabrication are discussed.

3.2.1 Polymethyl methacrylate (PMMA) Characteristics

PMMA, although being one of the first e-beam resists invented, is still the most commonly used high resolution EBL positive resist[17]. On exposure, the incident e-beam fractures the PMMA polymer backbone, creating a difference in the solubility properties of the exposed and unexposed areas [34]. PMMA was our choice as a positive resist for nano-size feature fabrication due to its extremely high resolution. Although its highest resolution is has been shown to be less than 10 nm in the literature [21], with the contribution of the PEC technique described above,

we could achieve better resolutions. In the literature, typical developer solutions for PMMA are 1:3 methyl isobutyl ketone (MIBK): isopropanol (IPA) and 1:1 MIBK: IPA. For our applications we preferred to work with 1:3 MIBK: IPA for its relatively high contrast in spite of its low sensitivity because resolution is the highest concern for nano-fabrication purposes [2].

3.2.2   Hydrogen Silsesquioxane (HSQ) Characteristics

HSQ has found applications as an interlayer dielectric material for integrated circuit implementations, and it is now used as a high resolution, negative tone e-beam resist [24]. It is commercially provided by Dow Corning under the name FOx (flowable oxide) with different concentrations of MIBK (FOx12 - FOx25) used as spinning solvent. HSQ is known to exist in three-dimensional forms of the monomer units of $H - SiO_{3/2}$. Different arrangements of these monomer molecules are observed before and after the curing. In figure 3.1 one of the most common model of HSQ structure (the cage model) is shown.
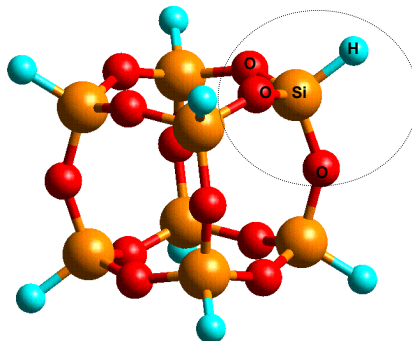

Figure 3.1: Most common HSQ cage model

Exposure in the HSQ resist system occurs as a result of the low activation energy needed to break the Si-H bonds and form much stronger siloxane (Si-O-Si) bonds. This chemical mechanism results in cross-linking; that is, these stronger siloxane bonds create smaller HSQ units and these smaller units attach to each other to form networks of long molecular chains, which lead to insolubility of the resist film on development. [24].Tetra-methyl ammonium hydroxide (TMAH) with a concentration of 2.38 % is the most commonly used developer for the HSQ applications. However, we preferred to use 25 % TMAH as a developer solution owing to its relatively higher contrast [15]. For our nano-fabrication purposes we preferred to work with FOx-14 in various dilutions due to its various proven advantages such as high resolution and satisfactory sensitivity.

3.3 Positive Resist Process

In positive resist processes, the main goal is to fabricate single layer metal structures with extremely high resolution in nanometer scale dimensions. Details of each step will be discussed below according to the process sequence illustrated in figure 3.2.

3.3.1 Substrate Preparation

We started the process by preparing the proper base to build our final devices. Silicon wafers are used as a supporting substrate for all the experiments. Since the operation of the ultimate device (nano-scale bow-tie antenna) requires to be

Perspective View   Front View

a.

nitride
oxide
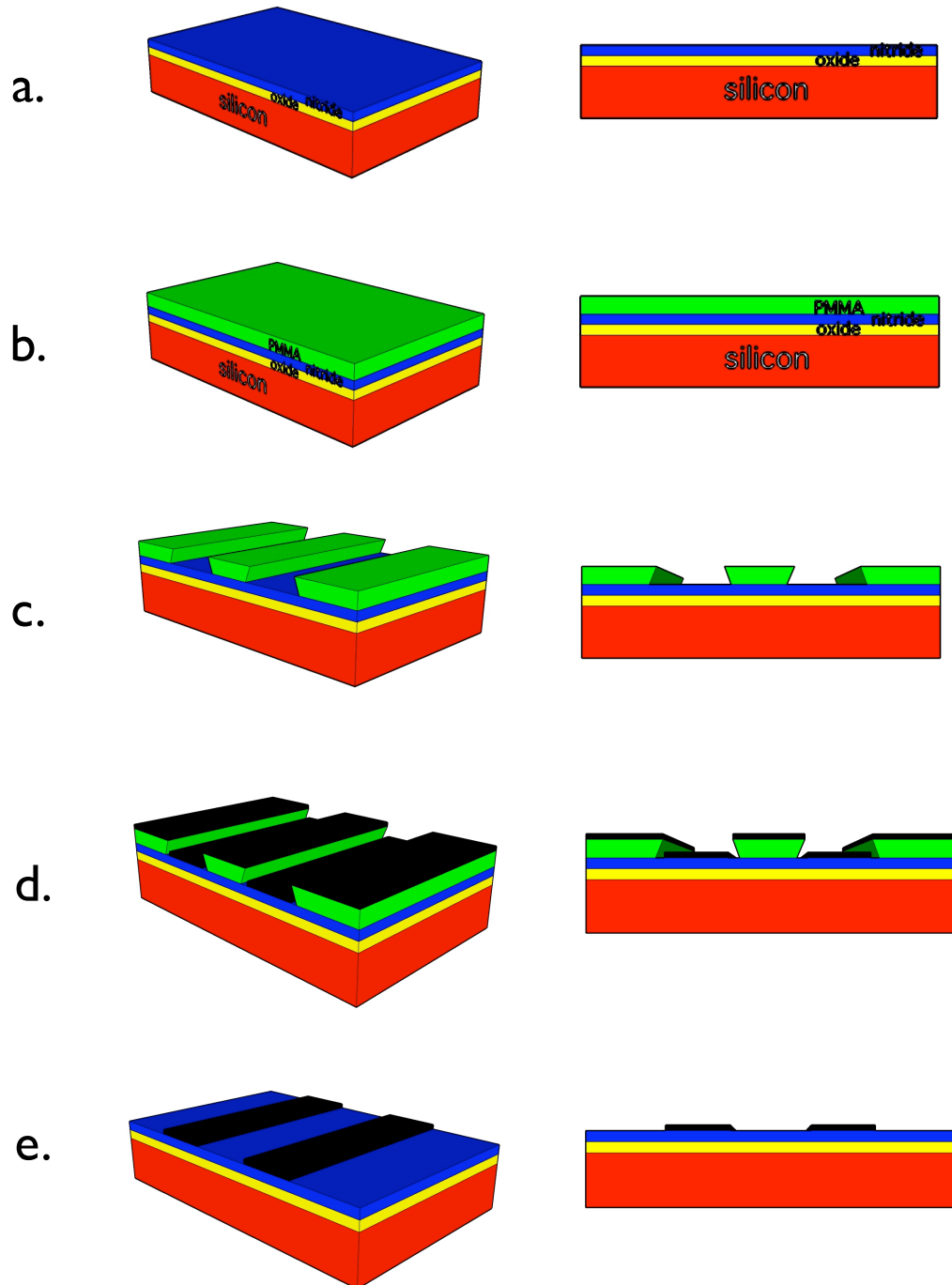silicon

b.

PMMA
nitride
oxide
silicon

c.

d.

e.

Figure 3.2: Positive resist general process flow

established on electrically well isolated basis, two isolation layers are deposited on this highly conductive silicon wafer. The first seal layer, a 100 nm thick silicon dioxide (SiO_2), is grown by dry oxidation in view of the fact that dry oxidation results in higher quality oxides. As a second isolation layer, 100 nm thick silicon nitride (Si_3N_4) is deposited on top of the oxide layer by low pressure chemical vapor deposition (LPCVD), considering that LPCVD will deposit high quality nitride material whose resistivity is high. The substrate described above can be seen in figure 3.2 a). After preparing the substrate, the 4" wafer is fractured into $1cm^2$ samples to be used for the rest of the process.

Working on a clean surface is one of the most important aspects of nanofabrication. In fact, performance of nano-sized bow-tie antennas is highly dependent on the smoothness of the surface. For this reason, prior to any process samples are cleaned in order to remove contaminants. The cleaning process is started by washing the sample with acetone for 1 minute on both sides. Next, methanol is used to wash the samples for another minute. The samples are blow dried with nitrogen before they are placed on a 120^0C hot plate for 5 minutes for the removal spinning solvent.

3.3.2   Resist Deposition

As stated, PMMA is used as our positive resist of choice. PMMA is commercially available in two formulas with molecular weights of 495K and 950K by Micro-Chem. In addition, each type comes with different dilutions in order to allow the deposition of a wide range of thickness at particular spin speeds. We spin

coated our samples with 495K- A4 type PMMA at 5000 revolutions per minute (RPM) expecting to achieve around 180 nm thickness relying on the film thickness vs. spin-speed curve plots provided by the commercial supplier. After the resist spin coating, a pre-bake process is applied by keeping the substrate on a 180^0 C degree hot plate for 90 seconds. As a result of the resist deposition step described above, the substrate can be seen in figure 3.2 b).

3.3.3   E-beam Exposure and Development

Raith e-LINE EBL tool uses thermal field emission filament technology and a laser-interferometer controlled stage. Beam energies between 100 eV and 30 keV are allowed. Also, six apertures are available in the system: 7.5, 10, 20, 30, 60, and 120 μm. In order to bring the forward scattering effects to a minimum, which is crucial for high resolution, we preferred to work with the highest energy beam provided by Raith e-LINE, which is 30 keV. Furthermore, a $30\mu m$ aperture size is selected in order to sufficient beam current current with this highly energized electron beam. We were able to reach a current level of 0.37 nA. Also, a 100 nm size writing field with a 10 nm step size is used in view of the fact that our patterns are always fractured into pixels that are not larger than 10 nm in size.

In order to develop the exposed resist, a solvent of 1:3 MIBK to IPA is used at room temperature for 50 seconds. As mentioned before this composition will allow the highest resolution, though will result in a very low sensitivity. Since the high resolution is of our highest interest, we compromised by accepting a low throughput.

The final view of our pattern after the e-beam exposure and development can be seen in figure 3.2 c).

3.3.4   Metal Deposition

After the desired pattern is accurately transferred into the resist media by EBL, the actual material that will constitute the final device is deposited. We chose to work with nickel due to its high conductivity as a metal, high corrosion-resistivity and relatively low cost. A 50 nm thin Ni layer is deposited using Denton e-beam evaporator. The fundamental mechanism of this particular metal deposition technique involves evaporation of the metal elements that move towards the target substrate and form a uniform thin layer. In fact, the evaporation occurs as a result of the energy accumulation on the source metal surface due to the high energy electrons' hitting the surface. The substrate looks as in figure 3.2 d) after the metal deposition.

3.3.5   Lift-Off

The last process step includes the removal of the resist layer together with the metal on top of the unexposed areas to achieve a finished product. This is realized by dissolving the resist in an organic solvent. We selected acetone at room temperature for the lift-off operation. At this phase of our process the most critical issue is metal tear-offs that happen during lift-off as a consequence of the junctions formed between the metal layers on the resist and the surface. There are several

factors affecting the success of the lift-off process. First of all, deposition should be directional and the surface of interest should be placed vertical to the incoming atoms. Secondly, the resist walls should not only be as vertical as possible but also some angle should be formed to create undercuts. We decided to use e-beam evaporation technique in order to create the directional deposition. In addition, we took advantage of the undercuts that happen as a result of using PMMA as a positive tone resist in order to prevent tear-offs.

3.4   Negative Resist Process Details

We use the negative-tone HSQ to explore subtractive (etch) processing. HSQ exhibits high etching resistance to enable the fabrication of nanometer-size bow-tie devices out of semiconductor materials through dry reactive ion etching (RIE.) Details of this process will be discussed below using the process sequence demonstrated in figure 3.3.

3.4.1   Substrate Preparation

The same substrate preparation described in the positive resist process is used in this process, except that an extra 60 nm thick poly-silicon layer is deposited on top of the nitride layer as shown in figure 3.3 a). This thin poly-silicon is doped by classic diffusion techniques. This conductive poly-silicon layer together with the negative tone e-beam lithography process allows the fabrication of structures that are made of conductive poly-silicon. For the substrate surface cleaning the same

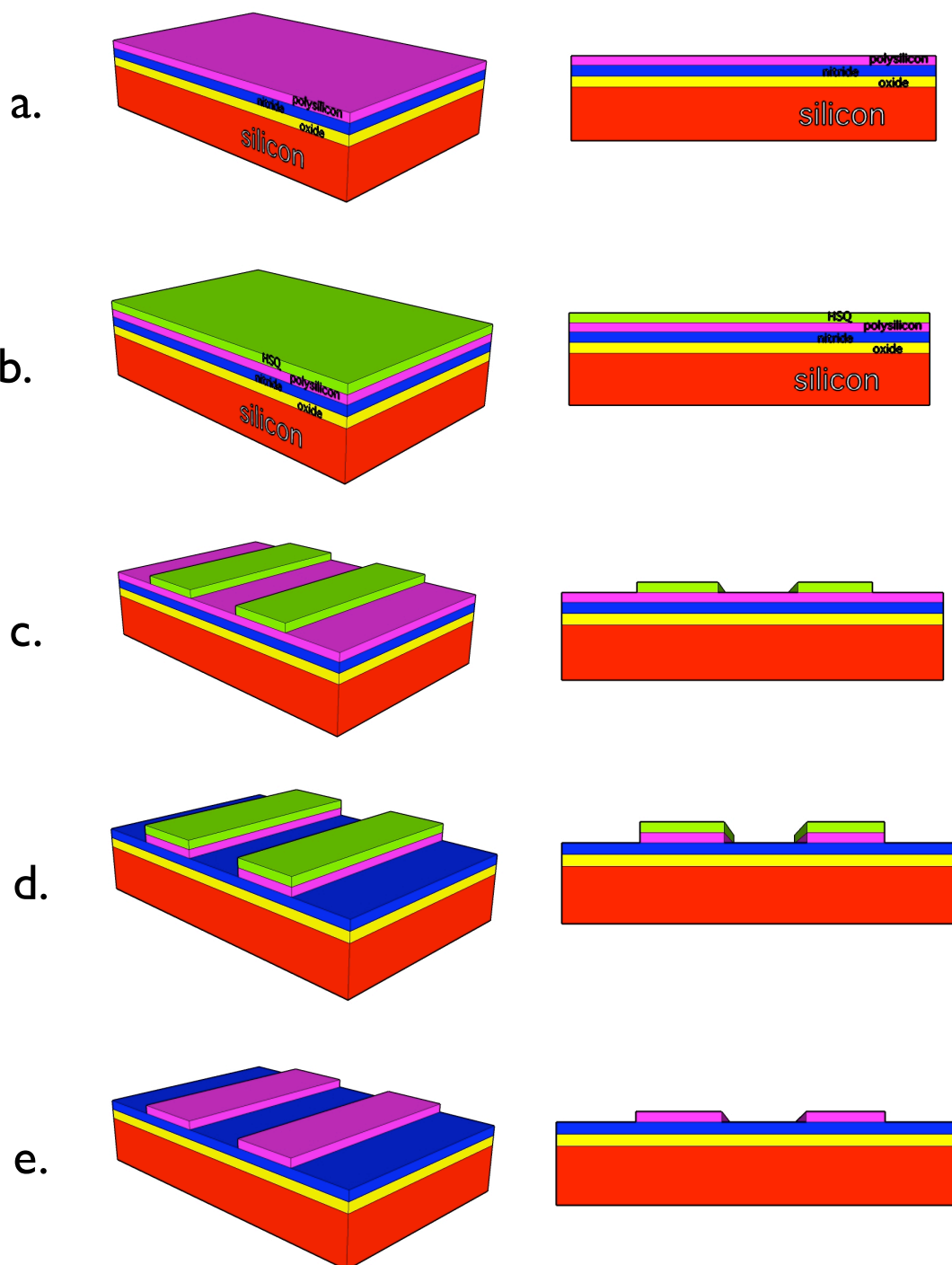## Perspective View   Front View

a.

b.

c.

d.

e.

Figure 3.3: Negative resist general process flow

procedure used as in the positive resist process.

3.4.2 Resist Deposition

We spin coated our samples with two different dilutions of FOx-14 with MIBK at 5000 RPM for 60 seconds. In the first case, the substrate is spin coated with pure FOx-14 in order to achieve around 200 nm thickness based on the film thickness vs. spin-speed curve plots provided by Dow Corning. In the second case the solvent of 1:1 FOx-14 to MIBK is used to spin coat the substrate in order to deposit a 100 nm thick layer of resist. After the resist spin coating, a two-step pre-bake process is applied by keeping the substrate on a 150^0 C degree hot plate for 2 minutes first and then on 200^0 C degree hot plate for another 2 minutes. The results of the resist deposition steps described above can be seen in figure 3.3 (b).

3.4.3 E-beam Exposure and Development

EBL is realized with the Raith e-LINE tool, whose properties were summarized above. Various acceleration potential and aperture size combinations were evaluated. In order to develop the exposed resist 25 % TMAH is used in order to achieve a high contrast. Development is realized at room temperature for 60 seconds. The final view of our pattern after the e-beam exposure and development can be seen in figure 3.3 c).

3.4.4 Etching

Once the desired pattern is transferred into the resist media, a proper etching method can be utilized to pass the resist template into the real material that we want the ultimate device to be made of. For our applications we used dry plasma etching. Although dry etching is directional (anisotropic), undercutting is inevitable in every etching process. In addition, this undercutting does not occur evenly at every part of the structure and changes character depending on the density of the pattern. This phenomena usually degrades our results and prevents us from observing the improvements due to PEC. Thus, we usually performed the comparison experiments taking the resist patterns as our basis before the dry etching is executed. However, if the ultimate goal is to create the real device, instead of merely making observations, dry plasma etching should be the best choice out of all the other subtractive fabrication methods. The substrate looks as in figure 3.3 (d) after the dry etching.

3.4.5 Resist Removal

In the last step resist is removed. For this, we dipped the sample into a Buffered Oxide Etchant (BOE) solution with the constitution of 1:10 HF to H_2O for 20 seconds. Then the sample is rinsed with water.

3.5 Imaging

During our experiments all the imaging is performed with Hitachi SU-70 Scanning Electron Microscope (SEM), which has an analytical ultra-high resolution field emission gun. This ultra-high resolution SEM has a resolution of up to 1 nm and, not only allowed us to inspect our nano-scale fabrication outcomes in great detail, but also guided us to determine optimum process parameters by supplying feedbacks during the experimental research. Below (in figure 3.4) a picture of the SEM system used is shown.

Figure 3.4: Hitachi SU-70 Scanning Electron Microscope (SEM)

Chapter 4

Results and Discussion

The results of our work will be presented in five sections. The first section involves the simulation results and the performance testing of the algorithm on various patterns. In the second part, negative resist process results are evaluated. Section three includes the positive resist process findings. In the forth section, the overall results will be evaluated and the extent of the objectives reached will be demonstrated while the shortcomings will be discussed and analyzed. Lastly, the fifth section is the conclusion.

4.1   Simulation Results and Performance Check of the Algorithm

Before presenting the implementation results, the simulation outcomes of the PEC using the linear programming algorithm will be demonstrated. The strengths and the weaknesses of this approach together with the performance check of it will be given.

4.1.1   Performance Analysis

As described earlier, one of the very valuable properties of this algorithm is that it informs the user of the maximum dose contrast possible for a given set of beam parameters. In other words, for every particular pattern and PSF function

there is a limit of edge contrast that can be achieved through mathematical methods and dose modulation approaches can, at most, achieve this contrast. In order to extract this information specific to our application, we determined the maximum achievable contrast for each pixel size (as it relates to beam diameter). In figure 4.1 the maximum achievable contrast is shown as a function of pixel size.
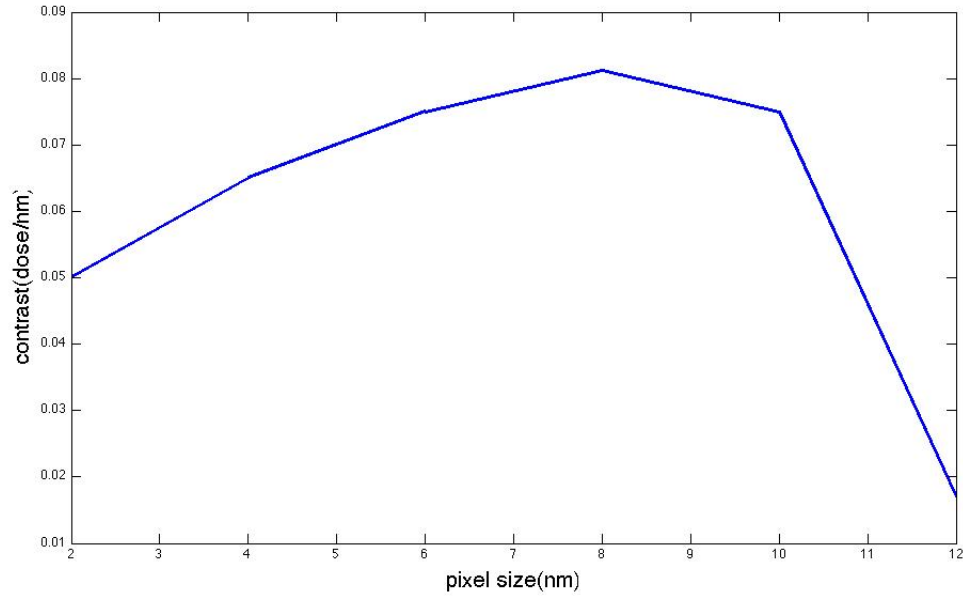

Figure 4.1: Maximum achievable contrast as a function of the pixel size

Execution time is major constraint on the implementation of this algorithm. This approach takes every pixel that defines the pattern as unknown and aims to assign a new dose value for each pixel that will satisfy the desired edge contrast. Therefore, computational processing time is strictly related to the size of the pattern matrix. Indeed, there are two dimensions controlling the process time: number of corrected pixels and the resolution requirement of the pattern. That is, a certain size pattern can be defined with various pixel sizes, which also determine the minimum

resolvable feature size and, also, the dimensional accuracy of feature reproduction.

Based on figure 4.1 and the process time limits, we decided to work with a 10 nm pixel size because, experience has shown, it is capable of providing the maximum achievable contrast and does not require extremely lengthly computer process time.

4.1.2   Simulation Results

In this section, the simulation results of the PEC algorithm are presented. These graphical outcomes make it easy to observe the difference between the modified and unmodified dose matrices. Also, 3-dimensional plots enable the comparison of accumulated dose profiles of the PE corrected and uncorrected patterns. Therefore, the evidence of the improvement in the absorbed dose edge slope is displayed.

The simulation results for the asymmetric bow-tie antenna pattern are given in figures 4.2 and 4.3. Dose matrices before and after the PE correction are shown in figures 4.2(a) and 4.3(a), respectively. It is clear in these plots that the deficiency of the accumulated dose at the corners and the edges are compensated by increasing the dose factors on these pixels so that the edge slope is increased in the modified cases. In figures 4.2(c) and 4.3(c) absorbed dose profiles for the corrected and uncorrected patterns can be found. The proximity-effect correction improvement in the edge slope of the absorbed dose profiles can be observed by looking at the color variations at the edges.
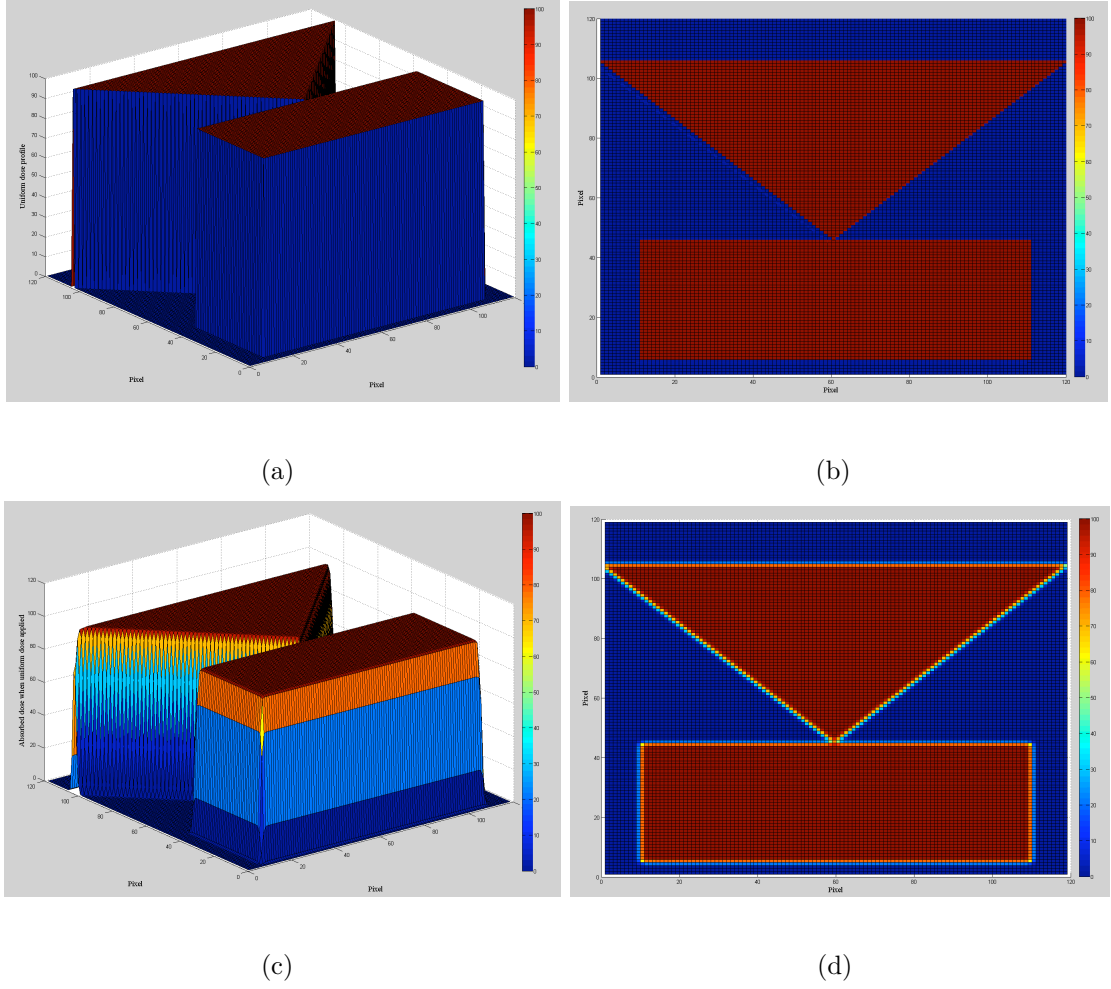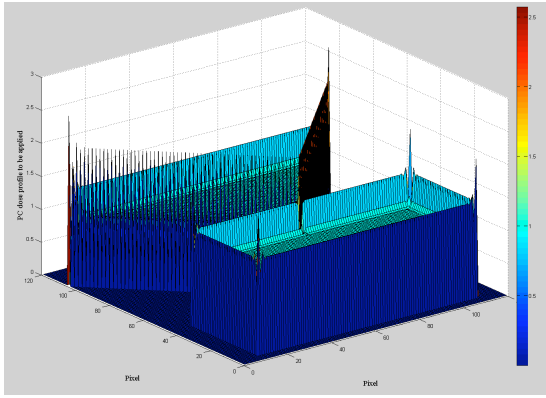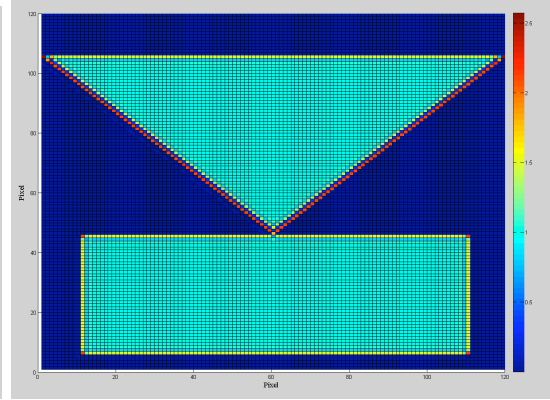
(a)

(b)

(c)

(d)

Figure 4.2: Simulation results without PEC: (a) Uniform dose profile; (b) Top view of (a); (c) Absorbed dose profile when uniform dose applied; (d)Top view of (c).

### 4.1.3 Simulation Results Under the Presence of Shot Noise

In this section effects of PEC in the presence of shot noise disturbances are discussed on the basis of the simulation results. In section 2.5.4 of this thesis, I propose, on a theoretical basis, that PEC improves the line-edge roughness created by shot noise. Increased edge slope of the accumulated dose profile created by PEC lessens the shot noise driven dose fluctuations.

(a)

(b)
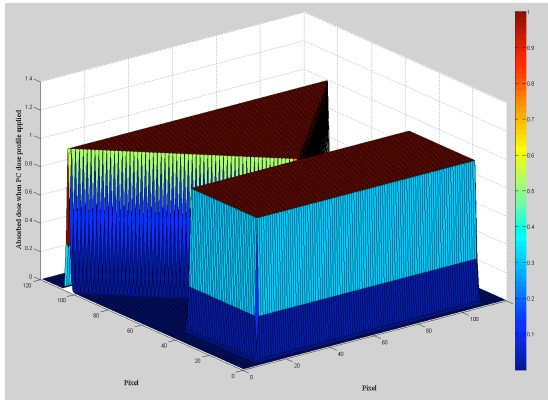
(c)
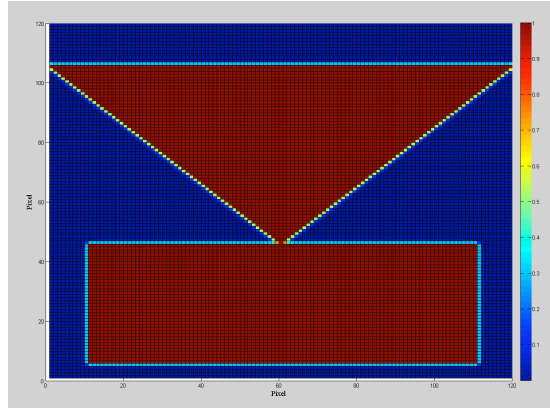
(d)

Figure 4.3: Simulation results with PEC: (a) PEC modified dose profile; (b) Top view of (a); (c) Absorbed dose profile when modified dose applied; (d)Top view of (c).

This phenomena is demonstrated on a simple square pattern. In figures 4.4(a) and 4.5(a) the uniform and the modified dose profiles are given, respectively. As a result of applying these dose profiles, the resulting total absorbed dose profiles, which can be seen in figures 4.4(b) and 4.5(b), are obtained. On the other hand, in figures 4.4(c) and 4.5(c) dose fluctuations due to shot noise is included in the dose profiles. It is clear in figures 4.4(d) and 4.5(d) that the dose fluctuations at the edge pixels are less effective in the PE corrected case due to the sharper edge slope.

(a)

(b)

(c)

(d)
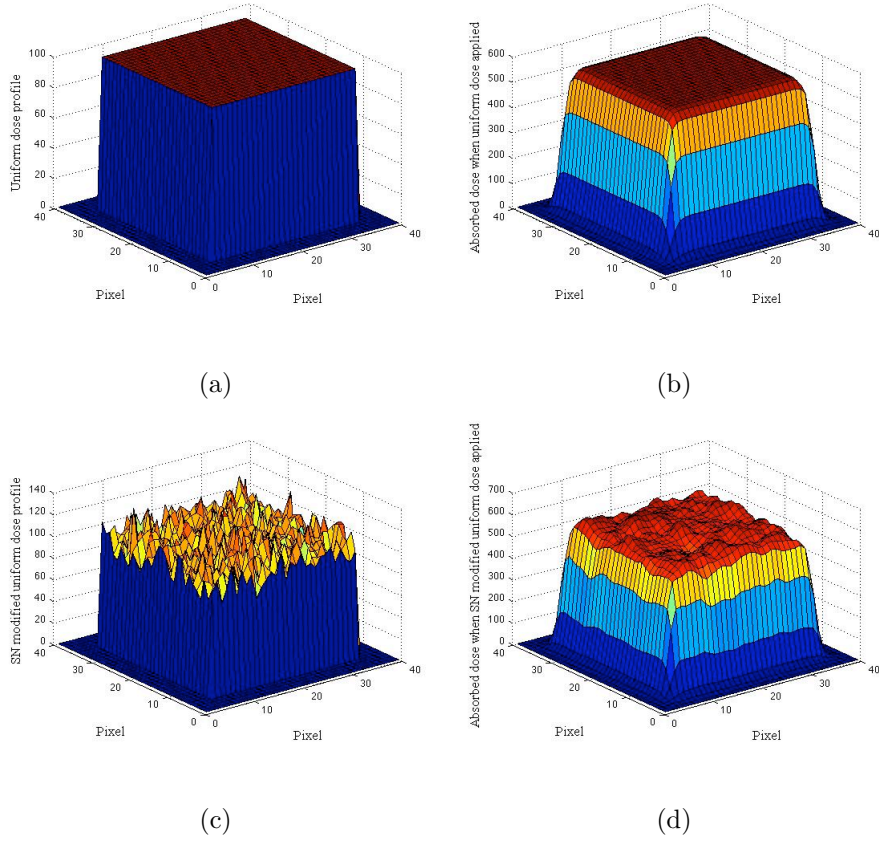
Figure 4.4: Simulation results without PEC: (a) Uniform dose profile; (b) Absorbed dose profile when uniform dose applied; (c) Shot noise included uniform dose profile; (d) Absorbed dose profile under the presence of shot noise.
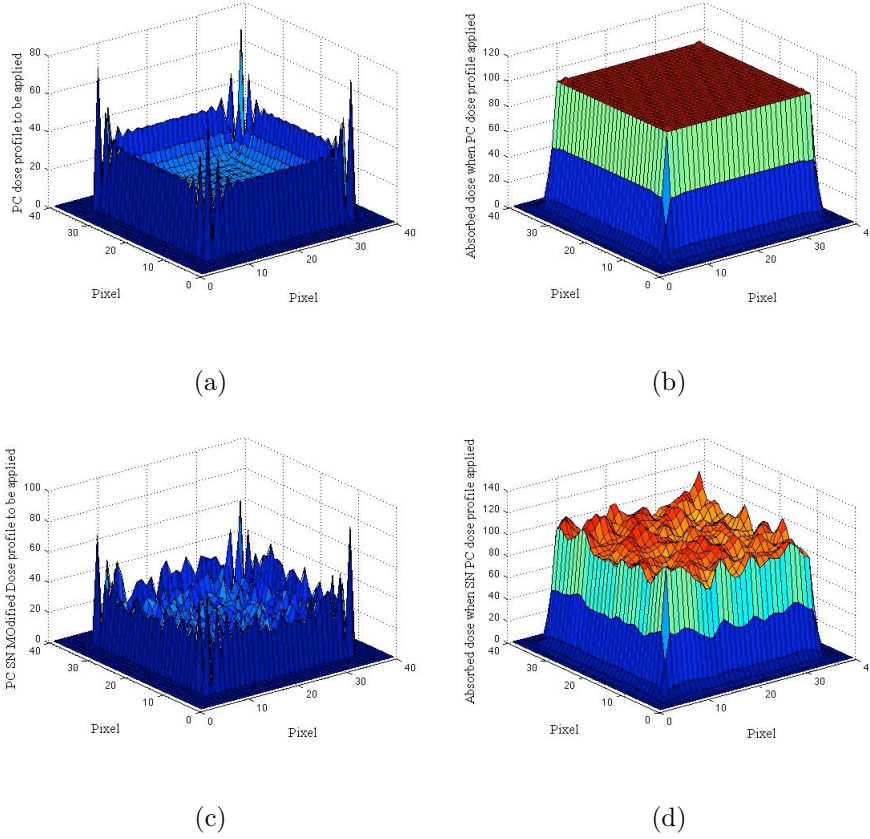
(a)

(b)

(c)

(d)

Figure 4.5: Simulation results with PEC: (a) PEC dose profile; (b) Absorbed dose profile when uniform dose applied; (c) Shot noise included PEC dose profile; (d) Absorbed dose profile under the presence of shot noise.

4.2 Negative Resist Process Implementation Results

As chemically-amplified negative resists are of great interest in e-beam lithography, we first used a negative resist process in our study of various approaches to proximity effect. Since negative resist HSQ remains dimensionally stable in the scanning electron microscope (as opposed to positive resist PMMA), we decided to use a negative resist process to observe the edge contrast right after resist development.

In figures 4.6, 4.7, 4.8 and 4.9, SEM images of the basic square patterns with

a 50° degree angle is shown. These tilted images enable the inspection of the edge slope characteristics of the modified and unmodified patterns. It is very clear in the figures that the PE corrected patterns show a very sharp edge slope while the uncorrected ones have a lot of distortion. In the figures the square patterns with $1\mu m$, 800 nm, 600 nm and 400 nm are presented. Although the performance was also checked for smaller patterns, SEM images for the smaller structures were not as clear because the required inspection angle decreased the SEM resolution.
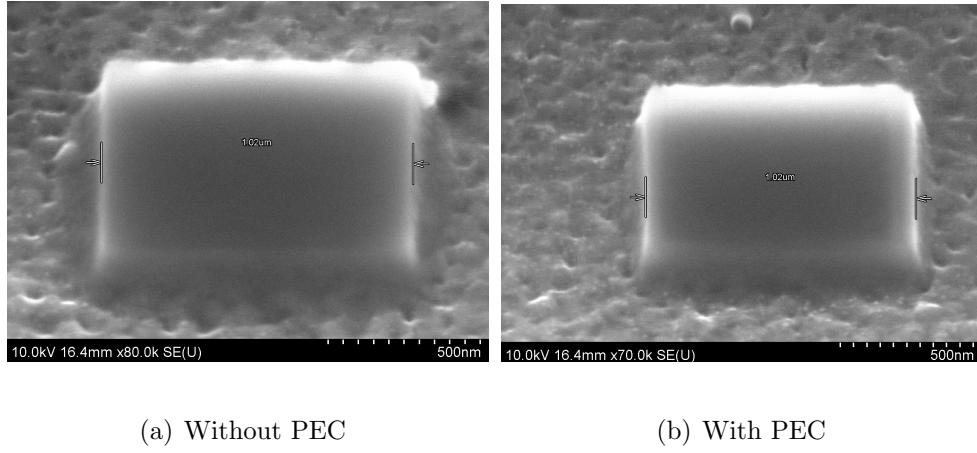

(a) Without PEC   (b) With PEC

Figure 4.6: SEM images of 1 um size square pattern with a 50^0 degrees tilt
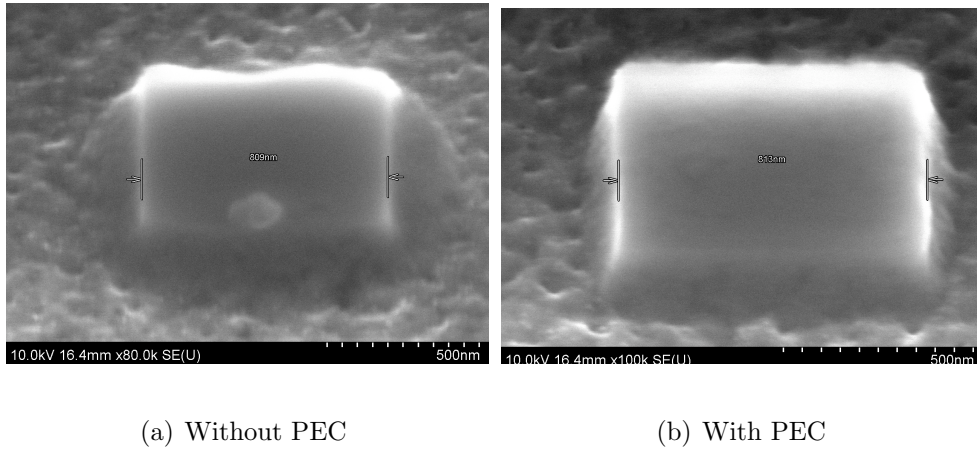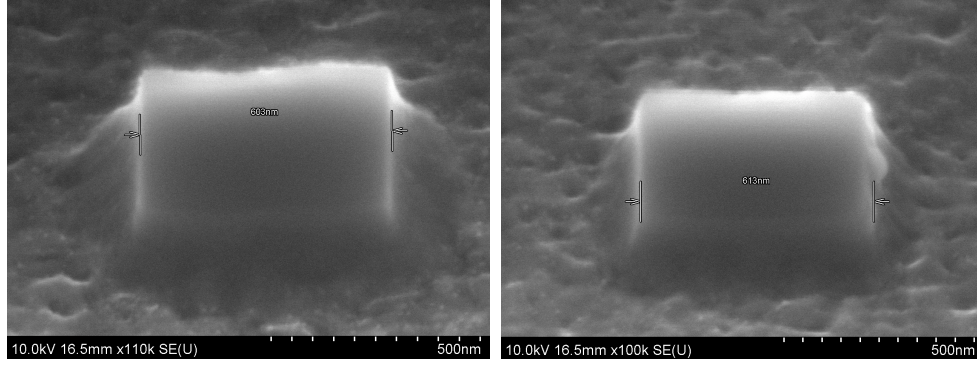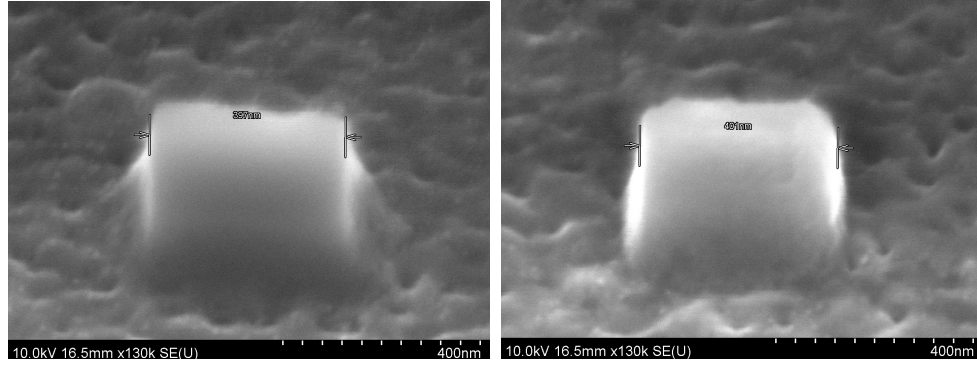

(a) Without PEC   (b) With PEC

Figure 4.7: SEM images of 800 nm size square pattern with a 50^0 degrees tilt

(a) Without PEC (b) With PEC

Figure 4.8: SEM images of 600 nm size square pattern with a 50^0 degrees tilt
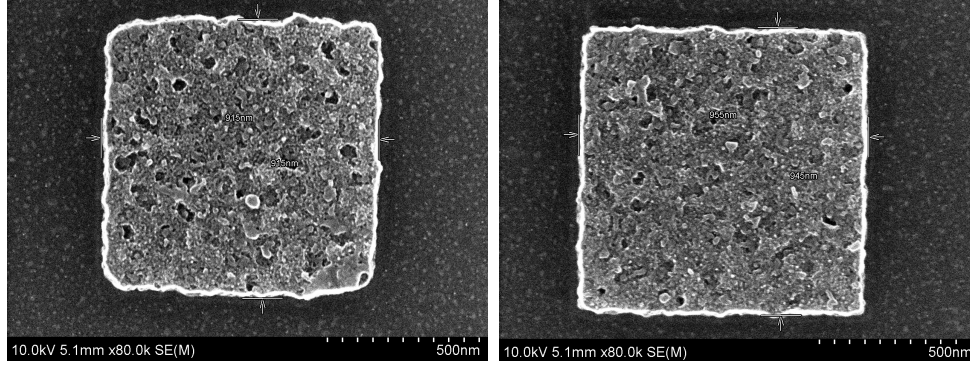

(a) Without PEC (b) With PEC

Figure 4.9: SEM images of 400 nm size square pattern with a 50^0 degrees tilt

This technique was also examined on polysilicon structures after RIE dry etching process. Figure 4.10 shows top views of simple square patterns with and without dose modification. These patterns are fabricated using the same base dose and identical mask size. The discrepancy in the two figures showcases the success of PEC. In addition to improvements in shape fidelity, such as sharper corners and smoother edges, the PE corrected pattern dimensions are in average, 3.5% closer to the actual mask dimensions.

(a) Without PEC   (b) With PEC

Figure 4.10: SEM images of 1um size square pattern of poly-silicon

4.3 Positive Resist Process Implementation Results

For the positive resist implementation purposes asymmetric bow-tie antenna pattern is used. In the fabrication of this specific pattern the most important challenge was the bridge forming in between the rectangle and the triangle antenna parts due to proximity effect problem. Although application of less amount of dose seems like a reasonable solution to sustain a gap in between the pattern portions, this results in underexposure. In other words, decreasing the dose to prevent the bridge formation fails because it either results in smaller structures or a complete distortion in shape fidelity. PEC with dose modulation technique was applied in order to beat these challenges.

4.3.1 Visual Results

In figures 4.11 - 4.13 the patterns after the dose modulation are shown. We were able to fabricate different structures with gap size less than 10 nm. The

structure in Fig. 4.11(a) stands out due to its small gap size: 2nm. In contrast, in figure 4.14 the best result achieved before the shape fidelity gets extremely distorted without PEC is given. Even though this device was fabricated with a dose 15% lower than the other structures, bridging persists.
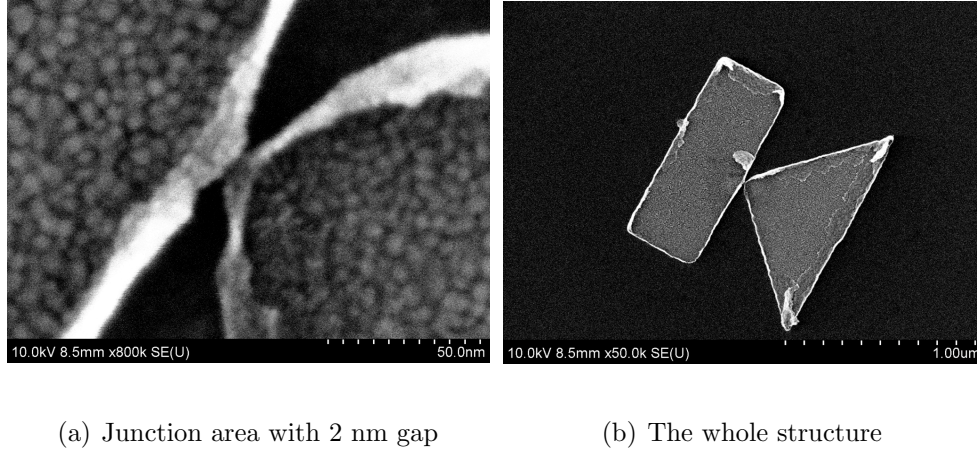

(a) Junction area with 2 nm gap

(b) The whole structure

Figure 4.11: SEM image of PEC, Ni, asymmetric antenna structure with 2 gap

(a) Junction area with 8 nm gap
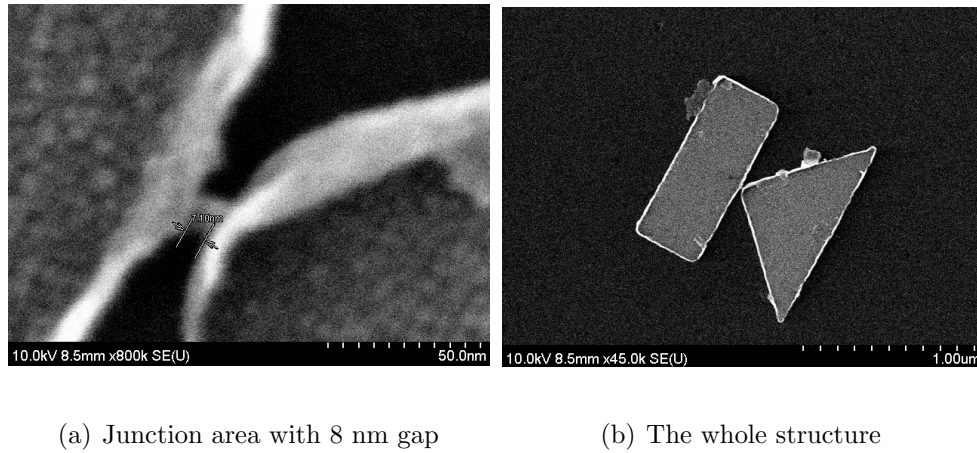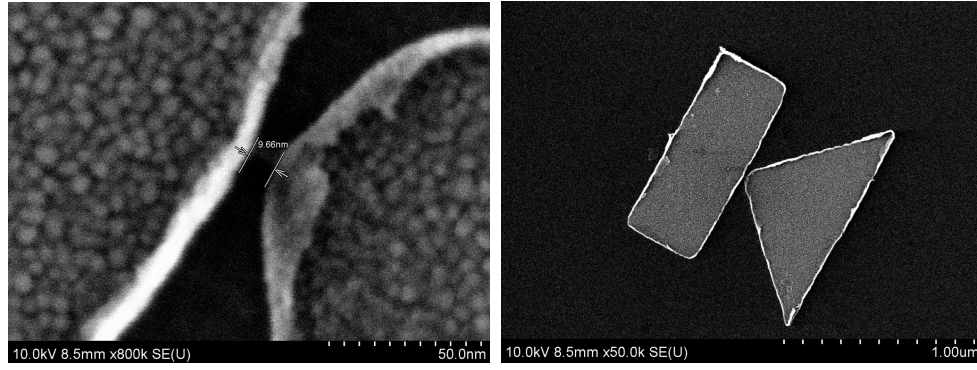

(b) The whole structure

Figure 4.12: SEM image of PEC, Ni, asymmetric antenna structure with 8 nm gap

We also used the commercially available RAITH PEC tool in order to compare the results we obtained using our PEC technique. Figure 4.15 shows two of the best results achieved with the RAITH software. In this structure, although the bridging

(a) Junction area with 10 nm gap (b) The whole structure

Figure 4.13: SEM image of PEC, Ni, asymmetric antenna structure with 10 nm gap
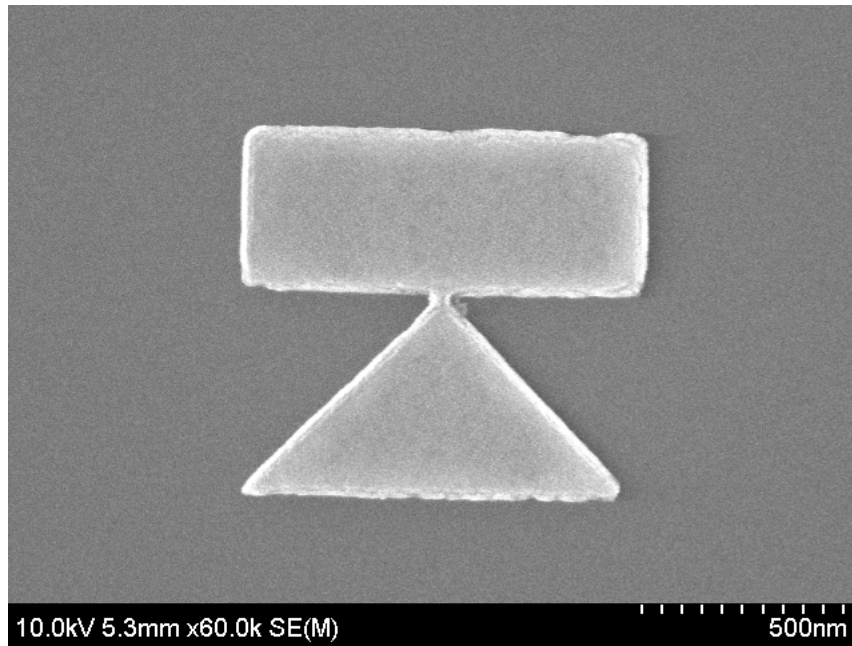

Figure 4.14: SEM image of Ni, asymmetric antenna structure fabricated without PEC

is not as wide as it is in the uncorrected pattern, the general shape fidelity is much poorer.
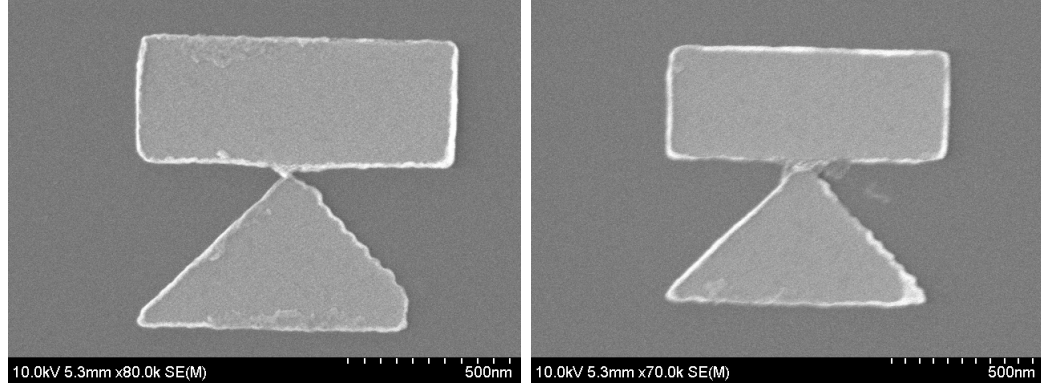
Figure 4.15: SEM images of the RAITH PE corrected asymmetric antenna structure

4.3.2 Numerical Results

The main objective of this work was to create a small gap size while keeping the structure size as close to the original design specifications as possible. In order to examine the results in terms of the specified objectives, the visual data obtained through the SEM images are analyzed numerically. The gap size and some relevant antenna dimensions are measured on the SEM images of structures that were created using different dose values and during the same fabrication process. Measurements are repeated for the antennas that are fabricated with and without PEC. Furthermore, three PEC methods, including two commercial ones and the one that employs linear programming (whose details were given in Chapter 2), are included in the numerical analysis and their performances are compared. These measurements were performed on structures created using dose values of 200 - 260 $\mu C/cm^2$. This dose range is significant because that is where the transition from gap to bridge occurs for all the techniques used.

The extents of the structure that are under consideration are shown in figure

4.16. Dimension A and B are the bottom edge and the height of the triangle, respectively. When C is positive, it represents the thickness of the bridge and when it is negative, it represents the width of the gap. In addition, dimension D stands for radius of curvature of the upper corner of the triangle.
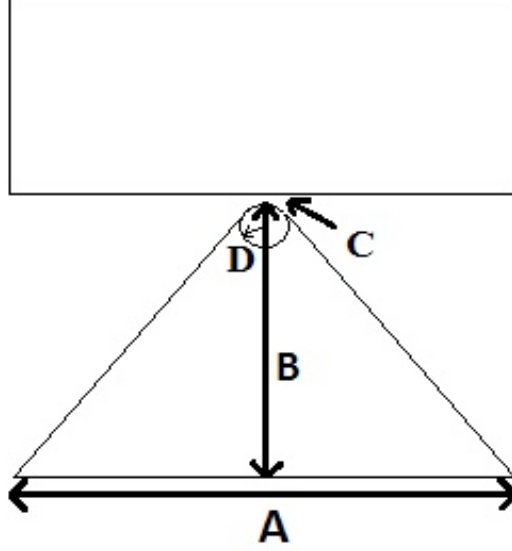

Figure 4.16: Relevant antenna dimensions

In Figure 4.17, the length of the bottom edge of the triangle (dimension A) is presented for the critical dose range (200-260). The ideal size of this dimension is 1180nm. This figure shows that Correction 1, which is PEC using LP, can result in structures that are closest in dimension to the original. On the other hand, the other commercial PEC techniques (Correction 2 and 3) fail to reach the ideal dimension at the same dose range. Furthermore, Figure 4.18 shows the measurements of the height of the triangle (ideal dimension = 600 nm) as a function of dose. It is clear from the figure that PEC with LP gives the best results as it is the closest to the ideal dimensions in the critical dose range.

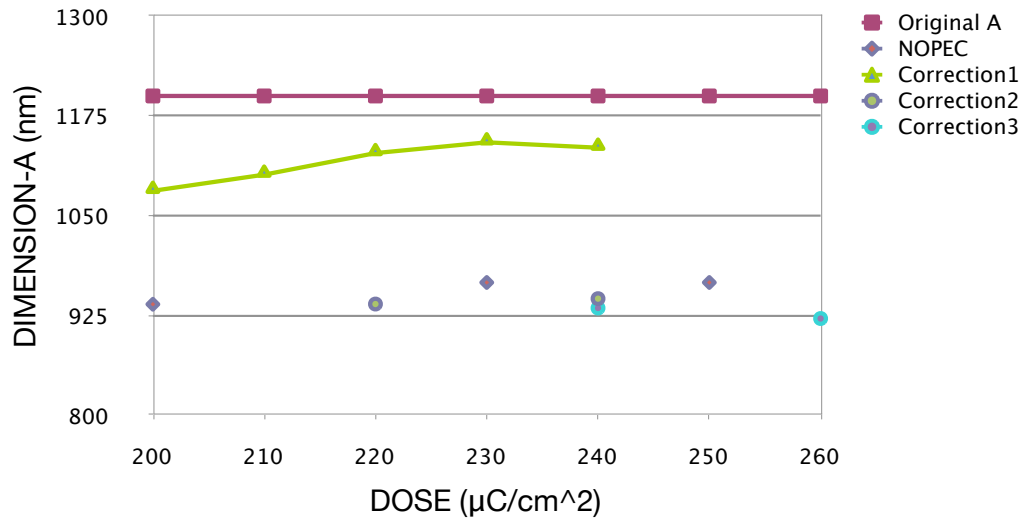Figure 4.17: Triangle bottom edge dimension (A) versus dose plots in cases of no correction and 3 different correction methods applied
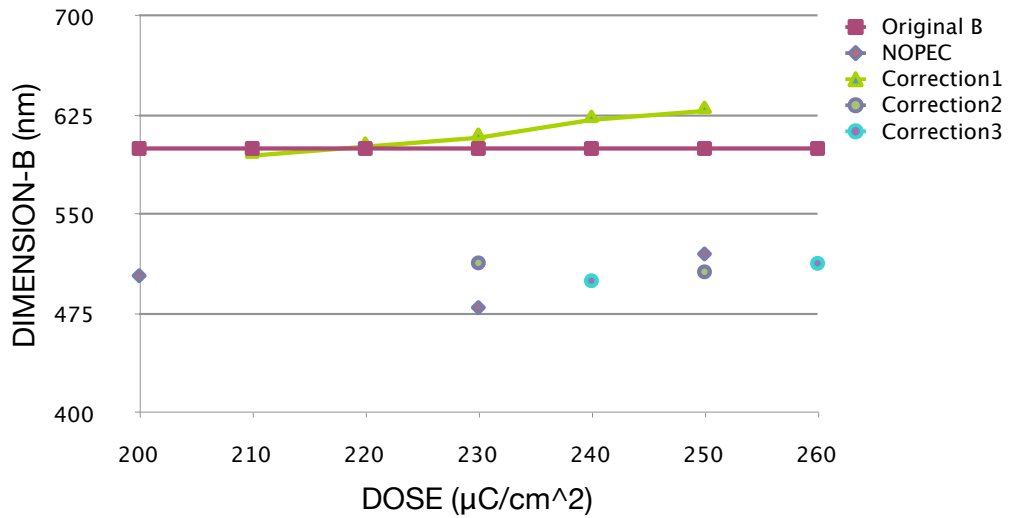

Figure 4.18: Triangle height dimension (B) versus dose plots in cases of no correction and 3 different correction methods applied

The measurements for the most challenging parameter, the gap size(dimension C), are shown in Figure 4.19. From this chart we can deduce that some techniques

(No PEC and Correction 3) form a bridge as soon as the dose value exceeds the exposure threshold of the resist. On the other hand, Correction 2 showed deformity at the gap and formation of a small sharp junction was not possible. The goal of a small gap was only achieved by Correction 1 (PEC with LP).
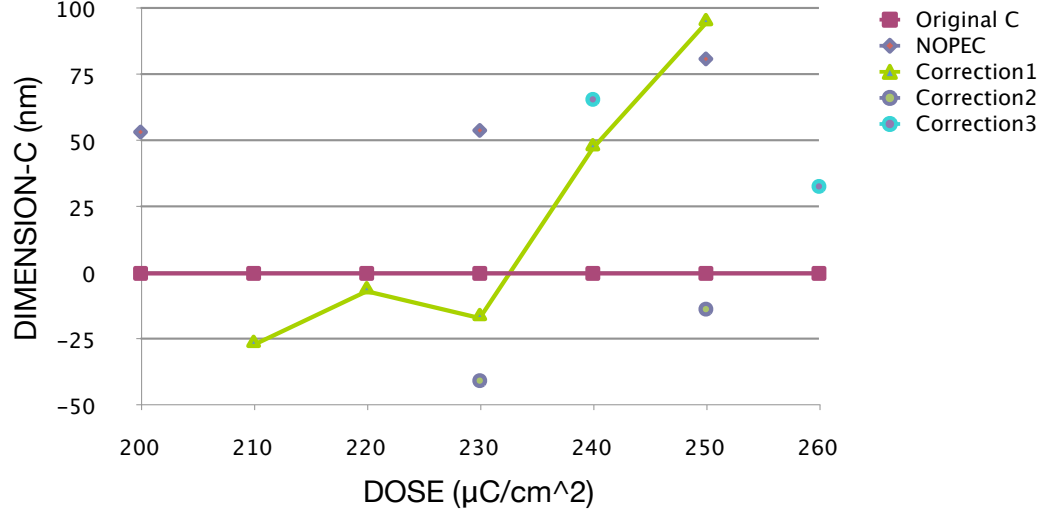

Figure 4.19: Gap dimension(≤ 0) or bridge dimension(≥ 0) versus dose plots for different correction methods applied

Another goal of this project was to form a minimum junction area. The radius of the curvature of the tip is measured to analyze this property. Figure 4.20 shows the radius of curvature of the samples created with Correction 1. The top corner of the triangle had its minimum($\sim$40 nm) when the minimum gap was formed.

In order to analyze the data further it was also necessary to observe the dimensional fidelity of the structures. In particular, we are concerned with edge roughness. An edge-detection algorithm called "Canny" provided by MATLAB was used. Several results obtained using this edge detector are presented in figure 4.21. Once the
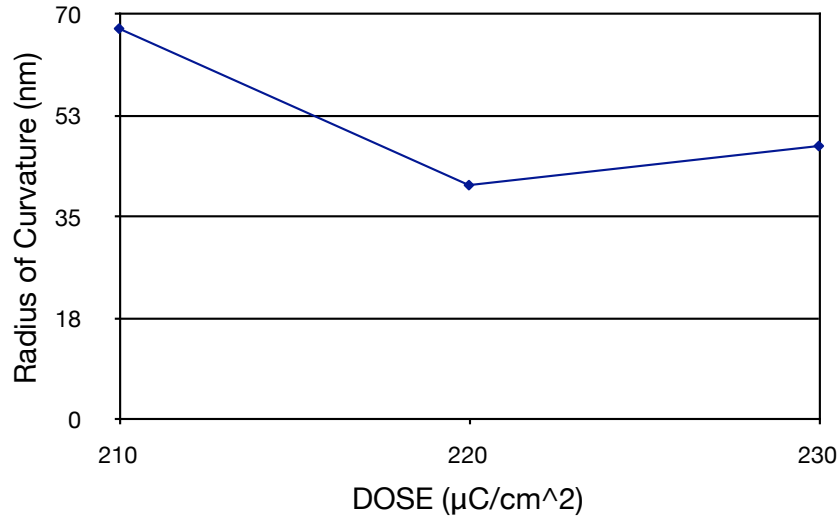
Figure 4.20: Radius of curvature versus dose plot for correction 1

edge data is extracted from the SEM images, a basic linear curve fitting technique
is applied on the edges that are under consideration. Deviations from the best lin-
ear fit for each edge are associated with the roughness. Root Mean Square Error
(RMSE) is used to quantify these deviations and so the edge roughness.

Figure 4.22 shows various results for the edge roughness analysis. In the first
row, findings for the lower edge of the rectangle in the asymmetric bow-tie patterns
that are generated at the same dose ($250\mu C/cm^2$) are given for the various methods.
It is clear from this data that Correction 1 produces a much lower deviation than
the uncorrected case, while the Corrections 2 and 3 provides worse result than
Correction 1, but still better than the not corrected case. In the second row, the
average RMSE values calculated on the same lower edge of the rectangle over a dose
range are given. Although there is a general trend of increase in the RMSE values
among the corrected cases, there is a decrease in the not corrected data compared
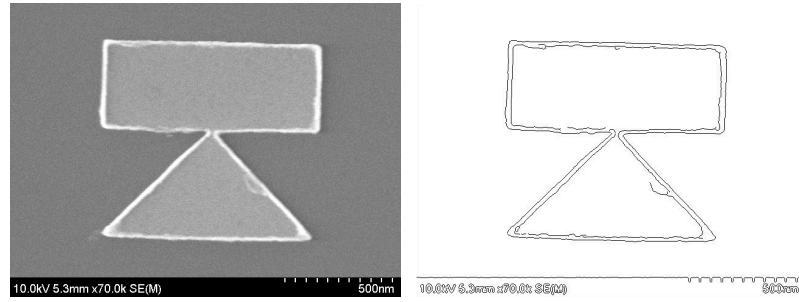
(a) SEM image and its corresponding edge data without PEC
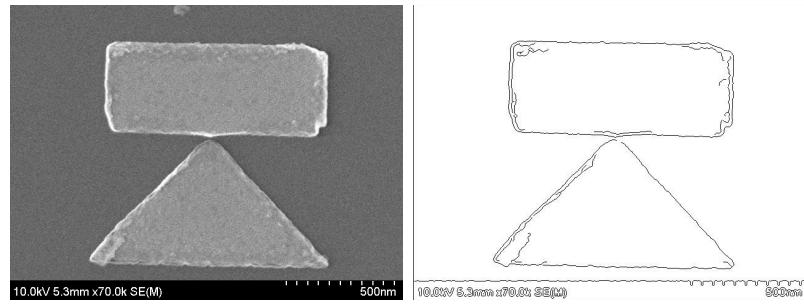
(b) SEM image and its corresponding edge data with correction 1
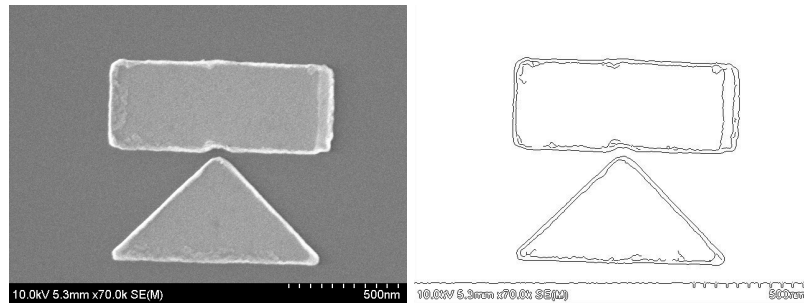
(c) SEM image and its corresponding edge data with correction 2

(d) SEM image and its corresponding edge data with correction 3

Figure 4.21: Edge detection results

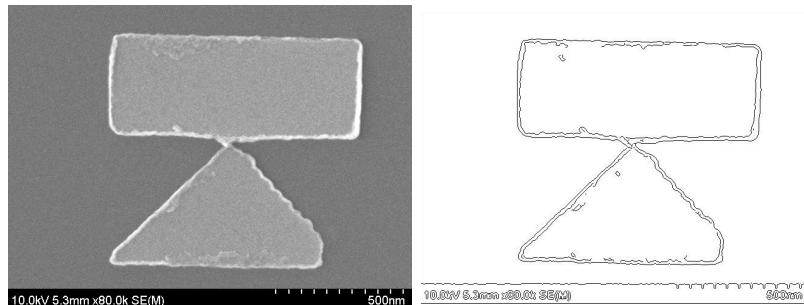| RMSE(nm)	NOPEC	Correction 1	Correction 2	Correction 3
identical edge, produced with the same base dose(250)	7.8433	1.9287	3.265	5.4067
identical edge, averaged over a dose range (200-260)	4.6710	2.5957	4.7390	7.5543
average of 3 outer edges, over a dose range (200-260)	3.3967	2.6640	3.4277	4.4650
average of 3 inner edges, over a dose range (200-260)	6.7707	5.9193	7.6533	5.4763
identical edge, at the optimum base dose of each technique	1.7020	1.4903	2.0440	1.8790

Figure 4.22: Edge roughness data table

to the first row. The worsening in the corrected pattern roughness can be explained by the dose dependence of the shape fidelity. As we are considering a dose range, underexposed and/or overexposed patterns tend to have a worse shape fidelity. Also, the reasoning under the improvement of the uncorrected pattern is data averaging over a dose range. Note that Correction 1 reveals less edge roughness in both cases.

In the edge detection plots usually two lines appear for each boundary: the outer representing the bottom edge and the inner representing the upper edge of the structure. The average RMSE values for each of these edges are also given in Figure 4.22, rows 3 and 4. Although Correction 1 gives the best results in both cases, the general trend gets worse for the inner edge because the lift-off process causes a lot of damage to the original pattern.

Lastly, a certain edge of the pattern is selected and the best result over all the doses used by each technique is compared in the last row of Figure 4.22. Here the RMSE values are observed to be very close to each other for both the corrected and

the uncorrected patterns, though Correction 1 still outperforms the others.

Considering all the numerical data presented above, we can conclude that PEC technique that uses linear optimization thrives in forming patterns that are most similar to the desired mask patterns by eliminating proximity effects. Moreover, this correction technique improves shape fidelity particularly on the edges that are facing the other patterns closely. However, it wasn't possible to observe a significant change in the edge roughness. This can be explained by the metal deposition and lift-off processes' effects. In the next section, the results presented above will be evaluated in light of of the objectives that were set at the beginning of this study.

4.4   Discussions

The first and the most important goal of this study was to create an air gap of size less than 5 nm in between the micro sized antenna segments (in the shape of a rectangle and a triangle) employing PEC techniques in order to enhance the resolution of EBL. This objective was satisfied. We were able to fabricate devices with gap sizes around 2 nm with the help of the PEC that uses linear programming techniques. However, the repeatability of this process was a big challenge due to the extremely small dimension requirements that are similar to the resolution limit of EBL. Indeed, the resolution limit is not a well-fixed number in EBL, because it is not simply determined by the device capabilities. That is, even though the device parameters are kept the same, slight changes in the other steps of the fabrication such as the substrate preparation, resist deposition and development conditions often

alter the EBL resolution. Therefore, repeatability required a strict control of the practical resolution limit, which is not easy to stabilize. Another challenge to achieve reproducibility came from the EBL device parameters, such as dose level. If it is aimed to produce nano-accuracy in the device dimensions, the dose threshold that results in the desired pattern becomes extremely crucial. It was a very demanding operation to detect the right dose amount for every specific process. And lastly, for each process EBL requires delicate parameter adjustments such as focusing, aperture alignment, beam alignment,etc. These parameters determine the beam shape, which is the most important external information that the PEC method takes as input. Thus, any distortion in the loop of the computation segment (PEC) and the practice (fabrication process) caused variations in the resultant device. In conclusion, although our objective was reached by showing the feasibility of PEC approach to obtain nano scale accuracy in EBL, other interferences mentioned above restricted the repeatability of the process.

Another very important goal of this study was set to keep the antenna dimensions fixed, while satisfying the gap size requirement. This goal was mostly satisfied by the alleviations done by PEC technique to the EBL. Without any PEC, the only procedure that would prevent bridge forming and give rise to gap formation is to keep the pattern underexposed by applying less dose than the required threshold. However, this results in smaller structures than the desired mask dimensions and a considerable distortion in the shape fidelity. However, PE corrected patterns generate structures whose properties are very similar to the actual mask requirements due to the improvements in the edge contrast of the accumulated dose. Thus, PEC

was very successful in maintaining the general pattern size requirements.

The small junction area requirement for the purpose of controlling the junction capacitance was also an objective of this work. In the corrected patterns, the smallest junction area was imposed by the smallest pixel size (10 nm) because the whole pattern is fractured to be able to apply dose modification. Therefore, in the corrected patterns junction area on the mask was not designed to be as sharp as the uncorrected pattern, which is made using a cat tool with a zero radius of curvature. As a result, PEC could not provide a significant improvement in terms of the corner sharpness of the patters.

4.5 Conclusions

The work presented in this thesis was motivated by the necessity of improving EBL resolution for the fabrication of asymmetric bow-tie antenna devices. These devices have been proposed as electromagnetic wave detectors and signal mixers in the literature. Fundamentally, they function as rectennas, accommodating two individual mechanisms: antenna and tunnel junction. The antenna couples the incident wave and forms an electric field enhancement between two antenna parts, while the tunnel junction employs this electric field, which is parallel to the charge transfer direction, to rectify the coupled wave and generates a DC output.

Our research not only aims to increase the speed of asymmetric bow-tie rectennas so that the operation frequency covers the IR-visible range of the spectrum, but also it has the goal of enhancing the detection efficiency to enable energy harvest

applications. The first goal was to design a planar structure so that surface plasmon resonance can contribute to field enhancement and improve the detection efficiency of the device. The second goal was to increase the speed of the device by creating a tunnel junction with a small barrier width and a small junction area in order to keep the RC bellow a certain threshold (and, thus, keep the cut-off frequency above a certain threshold). This goal, however, had the imposed constraint of maintaining the antenna dimensions constant. To satisfy these design criteria, a relative improvement in today's EBL resolution was necessary. Thus, substantial efforts were given to improve the performance of EBL by tackling its most common resolution problem: proximity effect. This was achieved by a dose modification technique that uses linear programming methods.

The performance of PEC was initially studied on simple patterns made of HSQ, a negative resist. SEM images were used to compare the edge slope difference between the corrected and uncorrected structures and the results were satisfactory. Secondly, the asymmetric bow-tie pattern was fabricated both with and without dose modification using a positive e-beam resist (PMMA), followed by a Ni lift-off process. In this process, two commercial PEC software packages were used in addition to the PEC that uses linear programming and the results were compared. We were able to fabricate Ni asymmetric bow-tie structures with a gap size less than 5 nm only on the samples where PEC using LP was employed. It was impossible to form a small gap without PEC. Also, since the other commercial correction methods were not designed for nano-accuracy, they showed deformation at the gap. In addition to the critical gap size, the actual pattern dimensions were only maintained on the

samples that were created by PEC using LP. Moreover, the effects of PEC on shape fidelity was studied in this thesis. Edge roughness information was extracted from SEM images using an edge detection algorithm. PEC using LP outperformed both commercial PEC techniques, particularly on edges that are close to other patterns.

Reproducibility was the only drawback of this process. Since the feature size we aimed to create required nano scale accuracy, it was difficult to control the process variations at each step of the fabrication. In conclusion, although our objective was achieved by proving that PEC can substantially increase the current EBL resolution, consistent reproduction was not possible.

The results we obtained revealed that the PEC technique that uses linear programming methods is currently the best solution for the prevention of the short range effects of the proximity problem in EBL. Therefore, this technique is applicable to lithography applications where nano accuracy is necessary.

Bibliography

[1] Feature contrast in dose-equalization schemes used for electron-beam proximity control. *Journal of Vacuum Science & Technology B: Microelectronics and Nanometer Structures*, 14:3880–3886.

[2] Gary H. Bernstein, Davide A. Hill, and Wen-Ping Liu. New high-contrast developers for poly(methyl methacrylate) resist. *Journal of Applied Physics*, 71(8):4066–4075, 1992.

[3] F.K. Kneubhl H. Rothuizen B. Lipphardt C. Fumeaux, W. Herrmann and C.O. Weiss. Nanometer thin-film ni-nio-ni diodes for mixing 28 thz co2-laser emissions with difference frequencies up to 176 ghz. *Applied Physics B: Lasers and Optics*, 66(3 / March):327–332, 1998.

[4] Allen M. Carroll. Proximity-effect correction with linear programming. *Journal of Applied Physics*, 52(1):434–437, 1981.

[5] T. H. P. Chang. Proximity effect in electron-beam lithography. *Journal of Vacuum Science and Technology*, 12(6):1271–1275, 1975.

[6] Richard Crandall, Uli Hofmann, and Richard L. Lozes. Contrast limitations in electron-beam lithography. volume 17, pages 2945–2947. AVS, 1999.

[7] J. W. Dees. Detection and harmonic generation in the submillimeter wavelength region. *Microwave Journal*, 9:48–55, 1966.

[8] Hans Eisenmann, Thomas Waas, and Hans Hartmann. Proxecco—proximity effect correction by convolution. volume 11, pages 2741–2745. AVS, 1993.

[9] S. Faris, T. Gustafson, and J. Wiesner. Detection of optical and infrared radiation with dc-biased electron-tunneling metal-barrier-metal diodes. *Quantum Electronics, IEEE Journal of*, 9(7):737–745, Jul 1973.

[10] J. C. Fisher and I. Giaever. Tunneling through thin insulating layers. *Journal of Applied Physics*, 32(2):172–177, 1961.

[11] J. S. Greeneich. Impact of electron scattering on linewidth control in electron-beam lithography. *Journal of Vacuum Science and Technology*, 16(6):1749–1753, 1979.

[12] Hongcang Guo, T. Zentgraf, T.P. Meyrath, Na Liu, Liwei Fu, S. Kaiser, H. Schweizer, and H. Giessen. Two distinct types of resonances in optical bowtie slot nanoantennas. In *Lasers and Electro-Optics, 2008 and 2008 Conference on Quantum Electronics and Laser Science. CLEO/QELS 2008. Conference on*, pages 1–2, May 2008.

[13] T. K. Gustafson, R. V. Schmidt, and J. R. Perucca. Optical detection in thin-film metal-oxide-metal diodes. *Applied Physics Letters*, 24(12):620–622, 1974.

[14] M. Heiblum, Shihyuan Wang, J. Whinnery, and T. Gustafson. Characteristics of integrated mom junctions at dc and at optical frequencies. *Quantum Electronics, IEEE Journal of*, 14(3):159–169, Mar 1978.

[15] W. Henschel, Y. M. Georgiev, and H. Kurz. Study of a high contrast process for hydrogen silsesquioxane as a negative tone electron beam resist. *Journal of Vacuum Science & Technology B: Microelectronics and Nanometer Structures*, 21(5):2018–2025, 2003.

[16] Uli Hofmann, Richard Crandall, and Leslie Johnson. Fundamental performance of state-of-the-art proximity effect correction methods. volume 17, pages 2940–2944. AVS, 1999.

[17] M. Hatzakis I. Haller and R. Srinivasan. High resolution positive resist for electron beam exposure. *IBM J. Res. Develop.*, 12:251–256, 1968.

[18] M. Dagenais K. Choi and M. Peckerar. Fabrication of thin film asymmetric tunneling diode using geometric field enhancement. *To be published*, 2009.

[19] Katja Keil, Marc Hauptmann, Kang-Hoon Choi, Johannes Kretz, Lukas M. Eng, and Johann W. Bartha. Fast backscattering parameter determination in e-beam lithography with a modified doughnut test. *Microelectronic Engineering*, 86(12):2408 – 2411, 2009.

[20] D. P. Kern. volume 80, page 326, 1980.

[21] Maroun Khoury and David K. Ferry. Effect of molecular weight on poly(methyl methacrylate) resolution. *Journal of Vacuum Science & Technology B: Microelectronics and Nanometer Structures*, 14(1):75–79, 1996.

[22] J. B. Kruger, P. Rissman, and M. S. Chang. Silicon transfer layer for multilayer resist systems. *Vacuum Science and Technology*, 19(4):1320–1324, 1981.

[23] Soo-Young Lee. A flexible and efficient approach to e-beam proximity effect correction - pyramid. *Surf. Interface Anal.*, 37:919–926, 2005.

[24] Hideo Namatsu, Yasuo Takahashi, Kenji Yamazaki, Toru Yamaguchi, Masao Nagase, and Kenji Kurihara. Three-dimensional siloxane resist for the formation of nanopatterns with minimum linewidth fluctuations. *Journal of Vacuum Science & Technology B: Microelectronics and Nanometer Structures*, 16(1):69–76, 1998.

[25] Morimi Osawa, Kimitoshi Takahashi, Masami Sato, Hiroshi Arimoto, Kozo Ogino, Hiromi Hoshino, and Yasuhide Machida. Proximity effect correction using pattern shape modification and area density map for electron-beam projection lithography. volume 19, pages 2483–2487. AVS, 2001.

[26] Geraint Owen. Methods for proximity effect correction in electron lithography. *Journal of Vacuum Science & Technology B: Microelectronics and Nanometer Structures*, 8(6):1889–1892, 1990.

[27] Geraint Owen and Paul Rissman. Proximity effect correction for electron beam lithography by equalization of background dose. *Journal of Applied Physics*, 54(6):3573–3581, 1983.

[28] Mihir Parikh. Corrections to proximity effects in electron beam lithography.(i. theory)(ii. implementation). *Journal of Applied Physics*, 50(6):4378–4382 and 4383, 1979.

[29] Mihir Parikh. Calculation of changes in pattern dimensions to compensate for proximity effects in electron lithography. *Journal of Applied Physics*, 51(1):705 – 709, 1980.

[30] J. M. Pavkovich. Proximity effect correction calculations by the integral equation approximate solution method. *Journal of Vacuum Science & Technology B: Microelectronics and Nanometer Structures*, 4(1):159–163, 1986.

[31] Martin Peckerar, Robert Bass, and Kee Woo Rhee. Sub-0.1 mu electron-beam lithography for nanostructure development. volume 18, pages 3143–3149. AVS, 2000.

[32] Martin Peckerar, David Sander, Ankur Srivastava, Adakou Foli, and Uzi Vishkin. Electron beam and optical proximity effect reduction for nanolithography: New results. volume 25, pages 2288–2294. AVS, 2007.

[33] P. A. Peterson, Z. J. Radzimski, S. A. Schwalm, and P. E. Russell. Low-voltage electron beam lithography. volume 10, pages 3088–3093. AVS, 1992.

[34] E Reichmanis and A E Novembre. Lithographic resist materials chemistry. *Annual Review of Materials Science*, 23:11–43, 1993.

[35] M. G. Rosenfield, S. A. Rishton, D. P. Kern, D. E. Seeger, and C. A. Whiting. A study of proximity effects at high electron-beam voltages for x-ray mask fabrication. i. additive mask processes. volume 8, pages 1763–1770. AVS, 1990.

[36] Eunsung Seo, Bo Kyung Choi, and Ohyun Kim. Determination of proximity effect parameters and the shape bias parameter in electron beam lithography. *Microelectronic Engineering*, 53(1-4):305 – 308, 2000.

[37] H. Sewell. Control of pattern dimensions in electron lithography. *Journal of Vacuum Science and Technology*, 15(3):927–930, 1978.

[38] J. G. Small, G. M. Elchinger, A. Javan, Antonio Sanchez, F. J. Bachner, and D. L. Smythe. ac electron tunneling at infrared frequencies: Thin-film m-o-m diode structure with broad-band characteristics. *Applied Physics Letters*, 24(6):275–279, 1974.

[39] L. Veneklasen, U. Hofmann, L. Johnson, V. Boegli, and R. Innes. Run-time correction of proximity effects in raster scan pattern generator systems. *Microelectron. Eng.*, 46(1-4):191–195, 1999.

[40] S. Y. Wang, T. Izawa, and T. K. Gustafson. Coupling characteristics of thin-film metal-oxide-metal diodes at 10.6 mu. *Applied Physics Letters*, 27(9):481–483, 1975.

[41] S. J. Wind, P. D. Gerber, and H. Rothuizen. Accuracy and efficiency in electron beam proximity effect correction. volume 16, pages 3262–3268. AVS, 1998.

[42] R. West. Proximity-effect induced density limitations for electron-beam patterned planar photonic nanomaterials. *Photonics and Nanostructures - Fundamentals and Applications*, 7(4):212 – 219, 2009. Mediteranean Nano Photonics 2008 (MediNano-1): Devices and fabrication techiques.

[43] Nanfang Yu, Ertugrul Cubukcu, Laurent Diehl, David Bour, Scott Corzine, Jintian Zhu, Gloria Höfler, Kenneth B. Crozier, and Federico Capasso. Bowtie plasmonic quantum cascade laser antenna. *Opt. Express*, 15(20):13272–13281, 2007.

[44] Jianyun Zhou and XiaoMin Yang. Monte carlo simulation of process parameters in electron beam lithography for thick resist patterning. *Journal of Vacuum Science & Technology B: Microelectronics and Nanometer Structures*, 24(3):1202–1209, 2006.